© 2020. Published by The Company of Biologists Ltd | Development (2020) 147, dev190082. doi:10.1242/dev.190082

RESEARCH ARTICLE

ENPL-1, the *Caenorhabditis elegans* homolog of GRP94, promotes insulin secretion via regulation of proinsulin processing and maturation

Agnieszka Podraza-Farhanieh[1], Balasubramanian Natarajan[2], Dorota Raj[1], Gautam Kao[1,*] and Peter Naredi[1,3,*]

ABSTRACT

Insulin/IGF signaling in *Caenorhabditis elegans* is crucial for proper development of the dauer larva and growth control. Mutants disturbing insulin processing, secretion and downstream signaling perturb this process and have helped identify genes that affect progression of type 2 diabetes. Insulin maturation is required for its proper secretion by pancreatic β cells. The role of the endoplasmic reticulum (ER) chaperones in insulin processing and secretion needs further study. We show that the *C. elegans* ER chaperone ENPL-1/GRP94 (HSP90B1), acts in dauer development by promoting insulin secretion and signaling. Processing of a proinsulin likely involves binding between the two proteins via a specific domain. We show that, in *enpl-1* mutants, an unprocessed insulin exits the ER lumen and is found in dense core vesicles, but is not secreted. The high ER stress in *enpl-1* mutants does not cause the secretion defect. Importantly, increased ENPL-1 levels result in increased secretion. Taken together, our work indicates that ENPL-1 operates at the level of insulin availability and is an essential modulator of insulin processing and secretion.

KEY WORDS: ER chaperone, Dauer, Dense core vesicles, Endoplasmic reticulum, Insulin secretion

INTRODUCTION

Type 2 diabetes (T2D) is a global health problem in which increased insulin resistance and deficiency in production of insulin by the pancreatic β cells are the key elements in the disease mechanism. Initially, the production of insulin is increased to maintain proper blood glucose levels; however, a continuous demand for insulin because of insulin resistance can lead to depletion of insulin production (Bell and Polonsky, 2001; DeFronzo, 2004). During insulin biosynthesis, the signal sequence of the preproinsulin is cleaved and the proinsulin enters the endoplasmic reticulum (ER). The proinsulin undergoes proper folding and formation of three pairs of disulfide bonds between the six cysteine residues in a fixed pattern, resulting in the final structure (Orci et al., 1986; Steiner et al., 2009). Proinsulin leaving the ER translocates to the Golgi apparatus and further into dense core vesicles (DCV), in which the propeptide is cleaved by the proprotein convertases 1/3 and 2 (Rhodes and Alarcon, 1994). When these conditions are met, the functional and mature insulin is secreted when the DCV fuses with the cell membrane in a tightly regulated manner. Although the processing of proinsulin and secretion of the mature insulin have been well described, much remains to be understood about the candidate proteins that are necessary for the proper handling of proinsulin in the cell and what are the candidate proteins that ensure the correct cysteine pairs form disulfide bonds.

GRP94 (also known as HSP90B1), a homolog of ENPL-1, along with GRP78 (BiP; Hspa5) and GRP75 (Hspa9), form a group of glucose-regulated proteins (GRPs) that are upregulated under low glucose conditions (Argon and Simen, 1999). GRP94 is a ubiquitously expressed protein mainly localized to the ER. However, a small fraction of this protein has been detected in the post-ER compartments such as Golgi (Frasson et al., 2009) and plasma membrane (Patel et al., 2013). GRP94 plays an essential role as a component of the ER quality control system, ensuring proper folding of secretory proteins (Argon and Simen, 1999), as well as in the detection of misfolded proteins during the ER-associated degradation (ERAD) (Christianson et al., 2008). GRP94 interacts with a limited set of client proteins, all of which are secreted, or integral membrane proteins. This includes integrins, toll-like receptors (Wu et al., 2012), as well as insulin-like growth factor (IGF) I and IGFII to ensure their proper maturation (Ostrovsky et al., 2009). The function of GRP94 is crucial in the organism, as the homozygous knockout in mice causes embryonic lethality (Mao et al., 2010) and the knockout in the pancreatic β cells in mice leads to impaired glucose tolerance and a diabetes phenotype (Kim et al., 2018).

In *Caenorhabditis elegans*, environmental challenges, such as nutritional supply, influence growth and metabolism via insulin/insulin-like growth factor signaling (IIS). IIS involves secretion of insulin/IGFs (Nakae et al., 2001). Genetic analysis performed in *C. elegans* suggests that the IIS pathway is activated by the binding of DAF-28, one of many agonistically acting insulin-like peptides, to the DAF-2 insulin receptor homolog and thereby controls growth and development by regulating the nuclear entry of the FOXO transcription factor DAF-16 upon activation of the PI3K/AKT lipid kinase pathway (Ogg and Ruvkun, 1998; Ogg et al., 1997; Zheng et al., 2018). Although the roles of insulin and IGFs in cell metabolism and growth have become better understood, mechanisms that regulate insulin maturation in worms are still unclear. A better understanding of this pathway involves the identification of previously unstudied proteins that influence insulin secretion.

[1]Department of Surgery, Institute of Clinical Sciences, Sahlgrenska Academy, University of Gothenburg, SE413 45 Gothenburg, Sweden. [2]Department of Surgical and Perioperative Sciences, Surgery, Umeå University, SE901 85 Umeå, Sweden. [3]Department of Surgery, Sahlgrenska University Hospital, SE413 45 Gothenburg, Sweden.

*Authors for correspondence (gautam.kao@gu.se; peter.naredi@gu.se)

A.P., 0000-0002-1120-8216; B.N., 0000-0003-2371-0550; D.R., 0000-0002-7357-2902; G.K., 0000-0003-1313-3024; P.N., 0000-0002-5652-0422

Handling Editor: Swathi Arur
Received 3 March 2020; Accepted 28 September 2020

Development (2020) 147, dev190082. doi:10.1242/dev.190082

In this study, we used *C. elegans* as a model organism to identify and characterize one such component. We describe the role of ENPL-1, the GRP94 homolog, in the regulation of DAF-28/insulin secretion. Our studies showed that lack of *enpl-1* leads to defects in the IIS activity. We showed that ENPL-1 binds to proinsulin/pro-DAF-28 and this binding requires the client binding domain of ENPL-1. We found that ENPL-1 is necessary to maintain proper insulin secretion and is sufficient to increase the insulin secretion process when overexpressed. The secretion of another neuropeptide is not affected in the mutants. Furthermore, we found that ENPL-1 is crucial for DAF-28/insulin biosynthesis and maturation, as the levels of DAF-28 were reduced significantly and DAF-28 remained in the unprocessed proinsulin form in *enpl-1* mutants. We also found that in *enpl-1* mutants, pro-DAF-28 can leave the ER lumen and likely is found in DCVs.

RESULTS

ENPL-1 is a broadly expressed protein localized to both ER and non-ER compartments

To study the localization of ENPL-1 in the worm, we used 3xFlag::ENPL-1 and CRISPR/CAS9 knock-in of super folder GFP (sfGFP) at the ENPL-1 locus. The 3xFlag::ENPL-1 transgene was inserted as a single copy transgene at another locus on chromosome 4. ENPL-1::sfGFP was broadly expressed throughout the animal, with strong expression in neurons, vulva, germline and intestine (Fig. 1A,B). To confirm the neuronal localization of ENPL-1, we co-expressed ENPL-1::sfGFP with a pan neural nuclear RFP and showed that ENPL-1::sfGFP is present in a peri-nuclear pattern characteristic of the ER (Fig. S1A,B). Furthermore, the expression of ENPL-1 was also observed at the early developmental stages in the embryo (Fig. 1B,C). Confocal analysis of ENPL-1::sfGFP worms co-expressing the mCherry tagged rough ER-specific marker SP12 (*spcs-1*) indicated that, as expected, ENPL-1 localized to the ER (Fig. 1D). Mammalian ENPL-1 homologs are found in non-ER locations in addition to the ER localization (Frasson et al., 2009; Patel et al., 2013). To ask whether this was the case for the worm ENPL-1, we used retrograde back filling of DiI into amphid neurons (Tong and Bürglin, 2010). We found that ENPL-1::sfGFP was present in the cell bodies of these neurons, where the rough ER and Golgi are found (Rolls et al., 2002), as well as in axons and dendrites, where there is no rough ER and Golgi (Fig. 1E). To further characterize the subcellular distribution of ENPL-1::sfGFP, we performed differential ultracentrifugation followed by western blotting, to separate and analyze membrane and cytoplasmic fractions. We discovered that ENPL-1::sfGFP is present in both the membrane and cytosolic fractions (Fig. 1F). Our analysis indicates that ENPL-1 is found mainly in the ER lumen; however, a fraction of the protein is present outside of the ER.

ENPL-1 is necessary for DAF-28/insulin secretion and is sufficient to increase insulin secretion

We have previously reported on an RNAi-based screen, which indicated *enpl-1* as a candidate gene to promote larval development and IIS in *C. elegans* (Billing et al., 2012). To investigate a possible role of *enpl-1* in insulin signaling we used two *enpl-1* mutants: *enpl-1(ok1964)* and *enpl-1(tm3738)*, which fully abolish gene (Fig. 2A) and protein (Fig. 2B) expression. The *enpl-1* mutations had severe consequences for the animal. The phenotypes included: sterility (Fig. 2C), body size defects and starved appearance (Fig. 2D), as well as cisplatin sensitivity (Natarajan et al., 2013). Depletion of *enpl-1* did not affect the general food intake as the pharyngeal pumping rate (Fig. S2A), the uptake of bacteria-sized fluorescent beads (Fig. S2B) and the uptake of fluorescence dye FM4-64 into the intestinal cells from the lumen (Fig. S2C) in *enpl-1(ok1964)* animals was comparable with the wild type.

We performed a series of genetic experiments to evaluate the IIS status of the mutants. First, we tested the subcellular localization of DAF-16::GFP/FOXO transcription factor, a well-established reporter of IIS activity (Henderson and Johnson, 2001). We found that 40% of the mutant animals had DAF-16::GFP in nuclei, in comparison with the complete cytoplasmic localization of DAF-16::GFP/FOXO in *enpl-1(+)* animals (Fig. 3A). Next, we tested the ability of *enpl-1* mutants to synergize with the reduced TGFβ pathway activity in *daf-7(e1372)* mutants to modulate dauer development, as reduced IIS function synergizes with a reduced TGFβ pathway to fully promote dauer formation (Ogg et al., 1997). At 15°C, 60% of the *daf-7(e1372);enpl-1(ok1964)* animals entered the dauer stage, compared with the 5% dauers in the *daf-7(e1372)* single mutants (Fig. 3B). To ask whether the enhanced dauer phenotype of *daf-7(e1372);enpl-1(ok1964)* requires *daf-16* function (Ogg et al., 1997), we created the triple mutant *daf-7(e1372);enpl-1(ok1964);daf-16(mgDf50)*. Our analysis revealed suppression of the *daf-7(e1372);enpl-1(ok1964)* dauer phenotype when *daf-16* function was eliminated (Fig. 3B). To test whether insulin secretion ability is perturbed in *enpl-1* mutants, we used the DAF-28::GFP/insulin reporter (Kao et al., 2007). We found that *enpl-1* is necessary for proper DAF-28/insulin secretion, as in the *enpl-1* mutants, secreted DAF-28::GFP was not found in coelomocytes, which are scavenger cells that take up secreted proteins accumulating in the pseudocoelomic fluid (Fig. 3C). Further, we tested the secretion of ANF::GFP, a non-insulin class neuropeptide (Speese et al., 2007), in the *enpl-1* mutants. Interestingly, the secretion of ANF::GFP to coelomocytes was not affected in the absence of *enpl-1*, indicating that the coelomocyte function was normal and that ENPL-1 might not affect the secretion of all classes of neuropeptides (Fig. 3D). In addition, mutations in another ER chaperone, *hsp-3(ok1083)*, which display high ER stress (Kapulkin et al., 2005), did not result in the insulin secretion defect, indicating that the DAF-28::GFP secretion defect is not a general feature of all ER-resident chaperones (Fig. S3A,B). Taken together, the results from DAF-16::GFP localization, enhancement of the dauer phenotype of *daf-7* mutants and blocked DAF-28::GFP secretion strongly supported the idea that IIS activity is low in *enpl-1* mutants. We concluded that ENPL-1 is a positive regulator of the IIS pathway.

To ask whether increased ENPL-1 levels might be sufficient to increase insulin secretion, we overexpressed ENPL-1 using a strain that expresses one extra copy of ENPL-1 tagged with 3xFlag-tag encoded by the transgene *knuSi222*, which was inserted at a different chromosomal locus. Our attempts to generate lines with multiple copies of the gene were unsuccessful. Expression of ENPL-1 from both its endogenous locus together with the transgene derived protein increased overall *enpl-1* mRNA (Fig. S4A) and protein levels (Fig. S4B), fully rescued the previously reported cisplatin phenotype (Natarajan et al., 2013) (Fig. S4C) and the sterility of the mutants (Fig. S4D). We found that overexpression of ENPL-1 in *knuSi222* worms (from the tagged and untagged proteins) was able to significantly increase the DAF-28::GFP/insulin accumulation in coelomocytes (Fig. 3E). Taken together, this *in vivo* analysis confirms that the ENPL-1 is necessary for insulin secretion and increased levels were sufficient to increase insulin secretion ability.

Improved ER folding capacity in neurons does not rescue the secretion block in *enpl-1* mutants

Chronically increased ER stress and increased ER stress-unfolded protein response (UPR^{ER}) activity negatively affects insulin

Development (2020) 147, dev190082. doi:10.1242/dev.190082

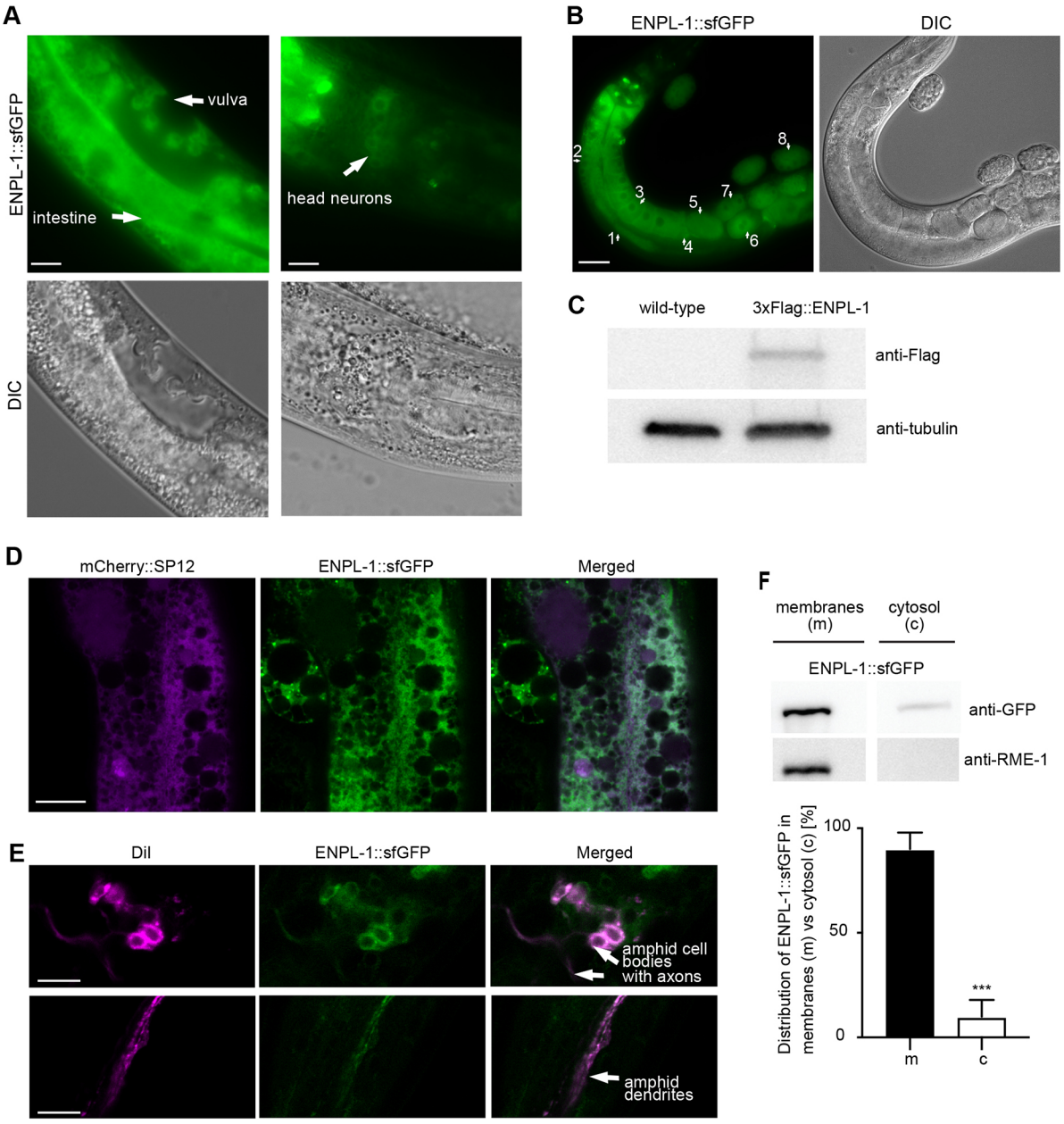

Fig. 1. ENPL-1 is broadly expressed and localizes to ER and non-ER cell compartments. (A) Representative fluorescence and differential interference contrast (DIC) images of 4th-larval-stage worms expressing ENPL-1::sfGFP. White arrows indicate different structures where ENPL-1::sfGFP is present. (B) Representative fluorescence and DIC images of embryos and adult *C. elegans* gonad expressing ENPL-1::sfGFP. Numbered structures are: (1) the rachis in the early germline; (2) older cellularized germ cells; (3) oocytes; (4) spermatheca; (5) one-cell embryo; (6) dividing one-cell embryo; (7) two-cell embryo; (8) embryos with multiple cells. (C) Western blot analysis of lysates prepared from wild-type and 3xFlag::ENPL-1 transgene-expressing embryos. The blot was probed with anti-Flag and anti-tubulin antibodies. (D) Representative confocal images of an int8 intestine cell expressing ENPL-1::sfGFP and the ER marker mCherry::SP12 ($n \geq 10$). (E) Representative confocal images of adult worms expressing ENPL-1::sfGFP and stained with DiI. White arrows indicate areas where DiI and GFP co-localize ($n \geq 10$). (F) Western blot analysis and quantification of ENPL-1::sfGFP in membrane (m) and cytosolic (c) fractions after ultracentrifugation. Blot was probed with anti-GFP and anti-RME-1 antibodies. The experiment was performed in triplicate. Statistical significance was determined by the two-tailed *t*-test (***P<0.001). Data are mean±s.d. Scale bars: 10 µm in A,D,E; 50 µm in B.

biosynthesis, leading to insulin secretion defects, pancreatic β cell dysfunction and development of diabetes mellitus (Kim et al., 2012). To understand how ENPL-1 regulates insulin secretion, we asked whether the lack of *enpl-1* caused increased ER stress. In *enpl-1(ok1964)* mutants, expression of the ER stress marker *hsp-4/BIP* was significantly upregulated compared with wild type (Fig. 2A) (Natarajan et al., 2013). It has been shown that the high ER stress in *ire-1(ok799)* mutants leads to the accumulation of DAF-28::GFP in the neuronal cell body, where the rough ER is present (Rolls et al., 2002), and blocks its exit from the ER towards dendrites and axons, thereby inhibiting insulin secretion (Safra et al., 2013). We found the same phenotype in *xbp-1(tm2457)* mutants (Fig. 4A). To understand whether the elevated ER stress levels of *enpl-1* mutants influenced transport of insulin from cell bodies to axons and dendrites, we analyzed DAF-28::GFP localization in ASI and ASJ neuronal cells. In contrast to *ire-1*

Development (2020) 147, dev190082. doi:10.1242/dev.190082

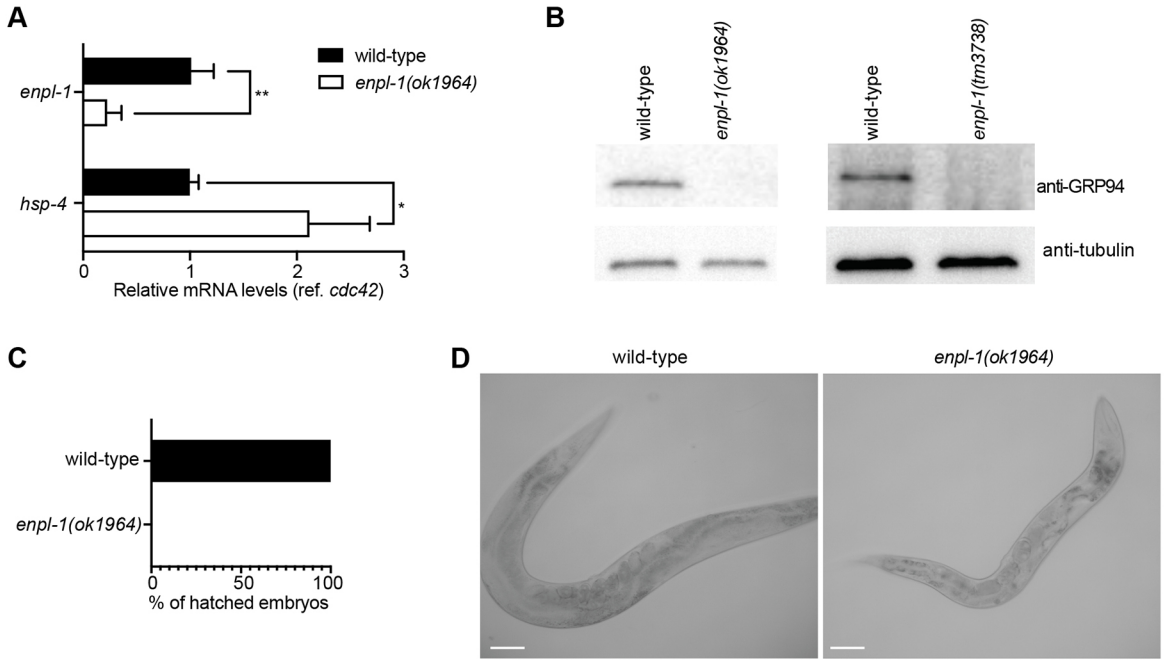

Fig. 2. *enpl-1* mutants have body size defects, inviable embryos and display high ER stress. (A) Relative qPCR analysis of *enpl-1* and the ER stress marker *hsp-4* expression in adult wild-type and *enpl-1 (ok1964)* mutants. Statistical significance was determined using the two-tailed *t*-test (**P*<0.05, ***P*<0.01). Data are mean±s.d. *cdc42* was used as a normalizing control for the experiment. The experiment was performed in triplicate. (B) Western blot analysis of ENPL-1 in wild-type animals, *enpl-1(ok1964)* mutants and *enpl-1(tm3738)* mutants. Blots were probed with anti-GRP94 antibody 9G10. Tubulin was used as a loading control. The 9G10 antibody recognizes *C. elegans* ENPL-1 protein. The experiment was performed in triplicate. (C) Quantification of hatched embryos 24 h after egg laying in wild-type and *enpl-1(ok1964)* mutants ($n \geq 50$). (D) Representative DIC images of adult wild-type and *enpl-1(ok1964)* animals of the same age. Scale bars: 100 µm.

and *xbp-1* mutants, in *enpl-1(ok1964)* mutants, DAF-28::GFP did not accumulate in the cell body and the transit through the ER to dendrites and axons was comparable with wild type (Fig. 4A). This indicates that the level or quality of ER stress in *enpl-1* mutants did not affect the transit of DAF-28::GFP through the ER to the post-ER compartments and that ENPL-1 is not needed for the exit of DAF-28/insulin from the ER. We conclude that the role of ENPL-1 in the process of insulin secretion might be more important at the post-ER levels.

One of the branches of UPR^{ER} activated by increased ER stress is the IRE-1/XBP-1 pathway (Calfon et al., 2002; Shen et al., 2001). The transcription factor XBP-1 acts downstream of IRE-1 to increase the production of ER chaperones and improve the folding capacity of the ER (Calfon et al., 2002; Klabonski et al., 2016). Overexpression of neuronally expressed and constitutively active *xbp-1* (*xbp-1s*) from the *uthIs270* transgene rescues tunicamycin resistance by increasing the expression of ER chaperones, indicating that the XBP-1s can be used to decrease ER stress (Taylor and Dillin, 2013). To ask whether improved folding capacity in the ER could suppress the *enpl-1(ok1964)* insulin secretion defect, we examined the *uthIs270;enpl-1(ok1964)* strain and did not observe any rescue of the DAF-28::GFP secretion defect (Fig. 4B). This indicates that improved chaperoning capacity in the ER lumen of neurons does not bypass the DAF-28::GFP secretion block in *enpl-1* mutants.

ENPL-1 regulates DAF-28/insulin expression and processing

To investigate the role of ENPL-1 in insulin processing and secretion we asked whether the transcriptional and translational levels of different insulin-type neuropeptides were affected by the absence of *enpl-1*. The qPCR analysis of three insulins, *daf-28*, *ins-4* and *ins-6* in *enpl-1* mutants showed that the transcriptional level of *daf-28* was significantly downregulated (Fig. 5A), whereas expression of the two other insulins, which belong to the same family of neuropeptides (Pierce et al., 2001), was not affected. (Fig. 5A).

To detect and analyze the processing of DAF-28 in *enpl-1(ok1964)* mutants, we created a double epitope-tagged DAF-28. The OLLAS tag was inserted in the F peptide, which is present only in the pro-DAF-28, and the MYC tag, which was inserted at the end of DAF-28. This reports on both the processed (mature) and the unprocessed (proinsulin) DAF-28/insulin (Fig. 5B). *daf-28* transcriptional level was significantly upregulated in the *ollas::daf-28::myc* expressing strain (Fig. S5A), as was expected for a multi-copy transgene. Western blot analysis of the otherwise wild-type strain detected pro-DAF-28 tagged with Ollas and Myc, as well as the mature processed DAF-28 tagged with only Myc (Fig. 5C). The DAF-28 protein produced by the transgene was biologically active as *ollas::daf-28::myc* could force dauer exit in *daf-7(−)* dauers at 25°C (Fig. S5B), as is the case for overexpressed untagged DAF-28 (Kao et al., 2007).

In *C. elegans*, processing of proinsulins to mature insulins requires the function of four proprotein convertases: AEX-5, BLI-4 and KPC-1, which are the homologs of human proprotein convertase 1 (PC1; PCSK1) (Thacker and Rose, 2000; Thacker et al., 2000), and EGL-3, which is a homolog of proprotein convertase 2 (PC2; PCSK2) (Kass et al., 2001). Proprotein convertases act in the dense core vesicles, in which the insulins are processed before secretion (Orci et al., 1986). Processing of pro-DAF-28 requires only the proprotein convertase KPC-1, which cleaves the proinsulin to remove the F peptide (Hung et al., 2014). We used the *kpc-1(gk8)* mutants to test whether *ollas::daf-28::myc* is indeed processed by the KPC-1. As expected, only

Development (2020) 147, dev190082. doi:10.1242/dev.190082

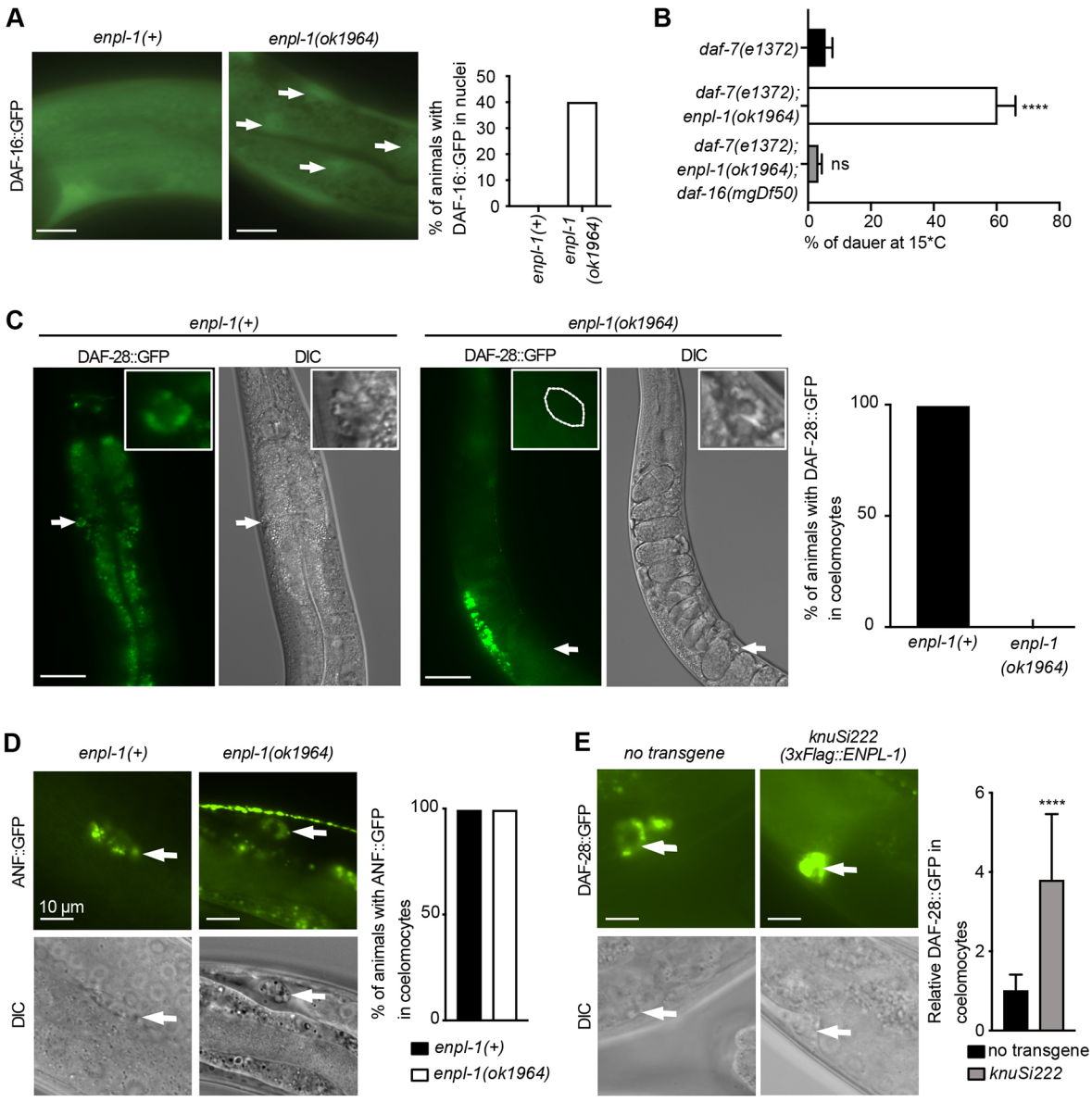

Fig. 3. ENPL-1 is necessary for maintaining proper DAF-28::GFP secretion and sufficient to increase DAF-28::GFP secretion. (A) Representative fluorescence images of adult *enpl-1(+)* animals and *enpl-1(ok1964)* mutants expressing DAF-16::GFP from the *zIs356* transgene. White arrows indicate nuclear localization of DAF-16::GFP. Quantification shows percentage of animals with DAF-16::GFP in nuclei ($n \geq 15$). (B) Quantification of the Daf-c dauer phenotype in animals of the genotypes *daf-7(e1372)*, *enpl-1(ok1964);daf-7(e1372)* and *enpl-1(ok1964);daf-7(e1372);daf-16(mgDf50)* at 15°C. Data are mean±s.d., percentage of dauer phenotype ($n \geq 40$). Statistical significance was determined using the two-tailed *t*-test (****$P<0.0001$). ns, not significant. The experiment was performed in triplicate. (C) Representative fluorescence and DIC images of adult *enpl-1(+)* animals and *enpl-1(ok1964)* mutants expressing DAF-28::GFP. White arrows indicate localization of coelomocyte in each animal. Insets (top right) show magnified fragment of animal with visible coelomocyte, dashed line shows DAF-28::GFP-negative coelomocyte. Quantification shows percentage of animals in which DAF-28::GFP is localized to coelomocytes ($n \geq 15$). (D) Representative fluorescence and DIC images of adult *enpl-1(+)* animals and *enpl-1(ok1964)* mutants expressing ANF::GFP. White arrows indicate ANF::GFP-positive coelomocytes. Quantification shows percentage of animals in which ANF::GFP is localized to coelomocytes ($n \geq 15$). (E) Representative fluorescence and DIC images of adult non-transgenic animals and *knuSi222(3xFlag::ENPL-1)* animals expressing DAF-28::GFP from the *svIs69* transgene. White arrows indicate DAF-28::GFP-positive coelomocytes. Quantification shows relative DAF-28::GFP fluorescence in coelomocytes, normalized to the non-transgenic strain, mean±s.d. ($n \geq 15$). Statistical significance was determined using the two-tailed *t*-test (****$P<0.0001$). The experiment was performed in triplicate. Scale bars: 15 µm in A; 50 µm in C; 10 µm in D,E.

unprocessed DAF-28 (pro-DAF-28) was detected in the *kpc-1(gk8)* mutant (Fig. 5C), thus validating the transgenic model. To ask whether the lack of *enpl-1* affects DAF-28 protein expression and processing we expressed *ollas::daf-28::myc* in the *enpl-1(ok1964)* mutant background. DAF-28 protein levels were decreased in *enpl-1* mutants (Fig. 5C). Furthermore, western blot analysis showed that the processing of DAF-28 was also affected in *enpl-1* mutants, as we could not detect the mature form of this insulin (Fig. 5C). Taken together, these data indicate that the expression of *daf-28* is influenced by *enpl-1*, and the maturation of DAF-28 neuropeptide requires ENPL-1.

Pro-DAF-28 binds to ENPL-1 and requires its conserved client binding domain region

As we observed that pro-DAF-28 was processed into DAF-28, we next asked whether this maturation event required a physical

Development (2020) 147, dev190082. doi:10.1242/dev.190082

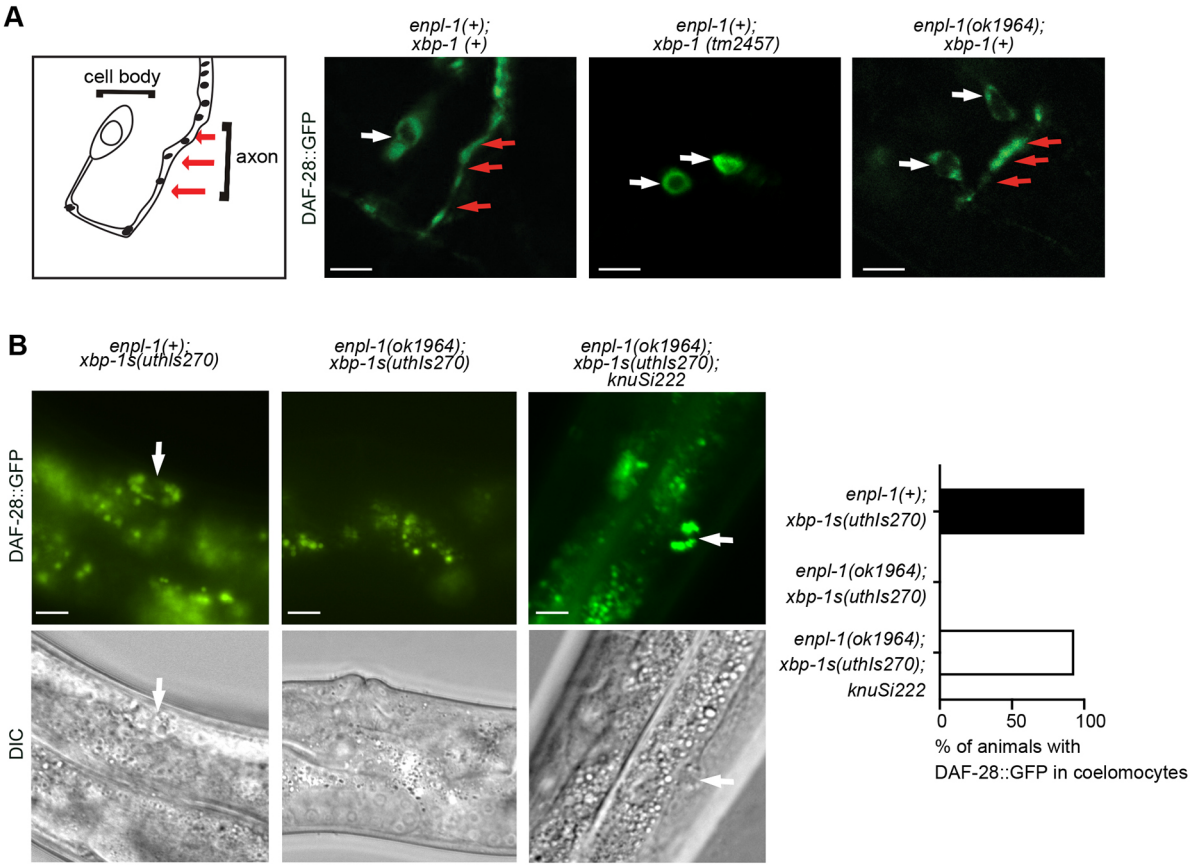

Fig. 4. Improved ER folding capacity in neurons does not rescue the secretion block in *enpl-1* mutants. (A) Schematic of amphid neurons with indicated cell body and axon (left) and representative confocal images of adult *enpl-1(+);xbp-1(+)*, *enpl-1(+);xbp-1(tm2457)* and *enpl-1(ok1964);xbp-1(+)* animals expressing DAF-28::GFP. White arrows indicate the neuronal cell bodies; red arrows indicate axons ($n \geq 10$). (B) Representative fluorescence and DIC images of adult *enpl-1(+)*, *enpl-1(ok1964)* mutant and *enpl-1(ok1964);knuSi222* co-expressing DAF-28::GFP and the neuronally expressed constitutively spliced form of XBP-1 from the *uthIs270* transgene. White arrows indicate DAF-28::GFP-positive coelomocytes. Quantification shows percentage of animals in which DAF-28::GFP is localized to coelomocytes ($n \geq 15$). Scale bars: 5 µm in A; 10 µm in B.

interaction between ENPL-1 and DAF-28. To analyze this, we generated a CRISPR knock-in of the mKate2 fluorescent protein just before the last four amino acids (HSEL) of ENPL-1. The expression pattern of ENPL-1::mKate2 was identical to that of ENPL-1::sfGFP including detection in all neuronal cells; confocal microscopy of *C. elegans* neuronal cells showed that ENPL-1::mKATE2 is expressed in the same cells as DAF-28::GFP and the two proteins co-localized (Fig. 6A). Co-immunoprecipitation followed by western blot analysis in a strain expressing *ollas::daf-28::myc* together with 3xFlag::ENPL-1 revealed that the tagged DAF-28 was found in the immunoprecipitate after the pull-down with the anti-Flag beads. This indicated that ENPL-1 can physically bind with the unprocessed *ollas::daf-28::myc* (Fig. 6B). To further understand how ENPL-1 binds to pro-DAF-28/proinsulin and which residues are necessary for the interaction, we deleted the highly conserved client-binding domain (CBD) of ENPL-1 in the 3xFlag::ENPL-1 strain (Fig. 6C). Although the 3xFlag:ENPL$^{\Delta CBD}$ protein levels were comparable with its wild-type epitope-tagged counterpart (Fig. S4E), the 3xFlag:ENPL$^{\Delta CBD}$ encoding transgene rescued neither the mutant sterility defect (Fig. S4D) nor the cisplatin sensitivity phenotype of *enpl-1(ok1964)* (Fig. S4C), even though 3xFlag::ENPL-1 fully rescued both these defects of *enpl-1(ok1964)* mutants (Fig. S4C,D). Co-immunoprecipitation experiments from worms expressing both 3xFlag::ENPL-1$^{\Delta CBD}$ and *ollas::daf-28::myc* revealed that the interaction between ENPL-1$^{\Delta CBD}$ and pro-DAF-28::Ollas was not detected, indicating that the ENPL-1 requires the client-binding domain to bind to the proinsulin (Fig. 6D).

Unregulated DCV release bypasses the secretion block of *enpl-1* mutants

To understand whether the *enpl-1* mutation affects DCV secretion ability, we analyzed the fluorescence levels and expression of transmembrane protein IDA-1::GFP, which spans the membrane of the DCV (Zahn et al., 2001). The levels of IDA-1::GFP were not affected in *enpl-1(ok1964)* mutants (Fig. 7A), indicating that the DCV levels were likely unchanged in *enpl-1* mutants. The *tom-1* (*tomosyn*) mutant, which causes unregulated DCV release and increases insulin exocytosis (Gracheva et al., 2007a; McEwen et al., 2006; Zhang et al., 2006), was further used. We found that the *tom-1(ok285)* mutant significantly increased DAF-28::GFP secretion (Fig. 7B), consistent with results from previously published work (Lee et al., 2011). Furthermore, we found that the severe insulin secretion defect of *enpl-1(ok1964)* mutants was partially bypassed in *tom-1(ok285);enpl-1(ok1964)* double mutants, as we detected DAF-28::GFP secretion in the coelomocytes of all animals (Fig. 7C). As DAF-28 is found only in the pro-form in *enpl-1* mutants, we asked whether the unprocessed form of DAF-28 can be secreted. To do this, we examined the secretion ability of DAF-28::GFP in *kpc-1(gk8)*

Development (2020) 147, dev190082. doi:10.1242/dev.190082

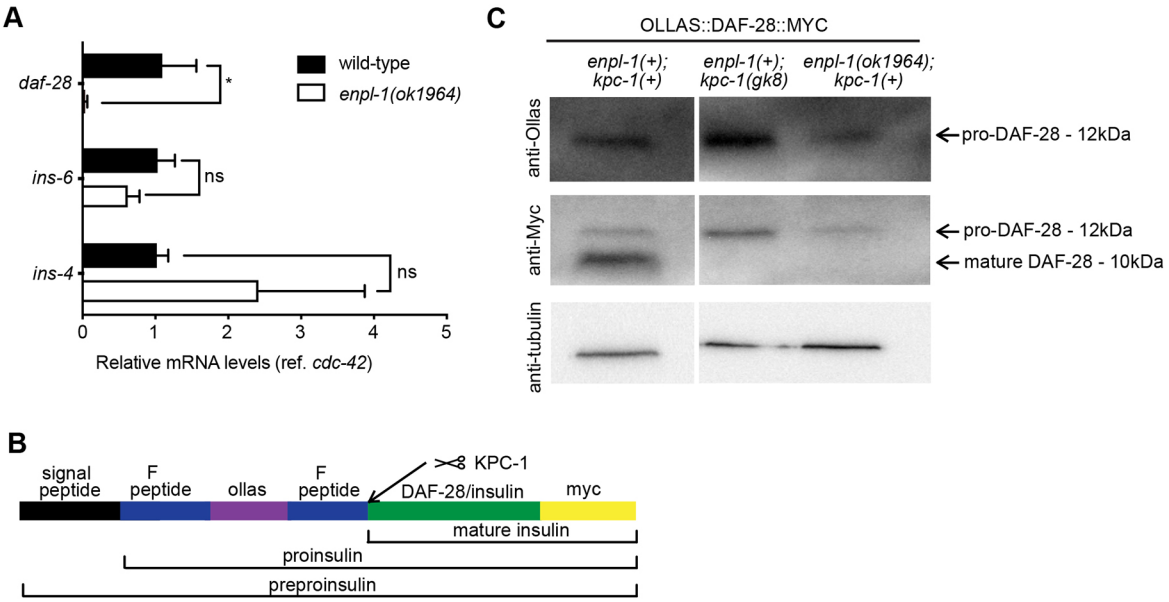

Fig. 5. ENPL-1 is required for DAF-28/insulin expression and processing. (A) Relative qPCR analysis of *daf-28*, *ins-6* and *ins-4* expression in wild-type and *enpl-1(ok1964)* mutants. Statistical significance was determined using the independent two-tailed *t*-test (*P<0.05). ns, not significant. Data are mean±s.d. *cdc42* was used as a normalizing control for the experiment. The experiment was performed in triplicate. (B) Schematic of OLLAS::DAF-28::MYC, with indicated positions of inserted OLLAS and MYC tags. The depicted protein domains are not to scale. (C) Western blot analysis of OLLAS::DAF-28::MYC in *enpl-1(+);kpc-1(+)* animals, *kpc-1(gk8)* mutants and *enpl-1(ok1964)* mutants. Blots were probed with anti-Ollas and anti-Myc antibodies. Tubulin was used as a loading control. The experiment was performed in triplicate.

mutants. As mentioned above, KPC-1 is necessary to process pro-DAF-28 and, in the absence of the enzyme, DAF-28 accumulates in the unprocessed form (Fig. 5C) (Hung et al., 2014). We found that DAF-28::GFP was secreted in *kpc-1* mutants (Fig. 7D); however, the secretion level was significantly decreased (Fig. 7D). Taken together, this analysis indicates that pro-DAF-28 reaches the DCVs in *enpl-1* mutants and the block in its maturation likely prevents the DCVs from releasing this cargo.

DISCUSSION

Here, we provide evidence that ENPL-1 is a new positive regulator of insulin signaling and insulin secretion in *C. elegans*. DAF-16::GFP is localized to nuclei in *enpl-1* mutants, the secretion of DAF-28/insulin::GFP is blocked and *enpl-1* mutants synergize with *daf-7(ts)* at the permissive temperature to enhance inappropriate entry into the dauer stage. Further, the overexpression with one extra copy of *enpl-1* is sufficient to elevate DAF-28/insulin secretion. This indicates that *enpl-1* is necessary for insulin secretion and sufficient to increase insulin secretion levels. ENPL-1 interacts with pro-DAF-28/proinsulin and this binding requires its client binding domain. We further found that ENPL-1 is necessary for proper conversion of pro-DAF-28 to processed DAF-28 and that DAF-28 levels are significantly lower in *enpl-1* mutants. Taken together, these various lines of evidence show that ENPL-1 acts at the level of DAF-28 in the IIS signaling cascade to stimulate IIS signaling in worms. We found that the elevated ER stress in *enpl-1* mutants does not contribute to the insulin secretion defect and that DAF-28::GFP exits the ER lumen properly in the mutants and likely reaches the DCVs.

Our previously published RNAi-based screening identified new genes that are involved in the regulation of IIS in *C. elegans* (Billing et al., 2012). Among the genes reported in that paper, we found that RNAi against *enpl-1* resulted in a larval growth arrest reminiscent of IIS defects (Billing et al., 2012). Previously, identification of mutants in genes that have a role in IIS was based on their ability to influence dauer development or affect the longevity (Fielenbach and Antebi, 2008). However, our approach allowed us to look for essential genes that impact IIS and cause sterility, primarily identifying *enpl-1* as an essential modifier of IIS in *C. elegans*. In addition, a study conducted in *Drosophila melanogaster* on the *Gp93* gene, an ortholog of ENPL-1, indicated that *Gp93* plays a crucial role in organismal development because the *gp93* mutation caused defects in larval midgut. Furthermore, *gp93* mutants exhibit a starvation-like phenotype and highly upregulated levels of the hemolymph trehalose. Both observations indicate suppressed insulin signaling pathway activity (Maynard et al., 2010). Our results agree with their findings, showing that the *enpl-1* gene is necessary for proper activity of the insulin signaling pathway. Here, we develop further the function of the gene in the insulin secretion process.

The genome of *C. elegans* encodes for 40 insulin-like peptides and only one insulin/insulin-like growth factor receptor DAF-2 (Pierce et al., 2001). We chose *daf-28* to study the secretion phenotype because its features indicate that it behaves functionally as an insulin. Previous work from our lab shows that secretion of DAF-28/insulin requires mitochondrial function (Billing et al., 2011). This is consistent with the studies in mammalian tissues, which show that the mitochondria metabolism controls insulin secretion from the pancreatic β-cells (Maechler, 2013). Another indication, that *daf-28* functionally resembles an insulin is a fact that its secretion is affected by mutants in DCV components. Insulins, but not IGFs, are packed into DCVs before secretion, and mutants in DCV components, such as *unc-31* or *tom-1*, affect DAF-28::GFP secretion (Lee et al., 2011). In addition, INS-6, which functionally resembles DAF-28 (Hung et al., 2014), can bind to and activate the human insulin receptor, with greater affinity than other reported analogs of human insulin (Hua et al., 2003). Confirmation of this notion is provided by our studies of mouse ASNA-1 (Get3; Norlin

Development (2020) 147, dev190082. doi:10.1242/dev.190082

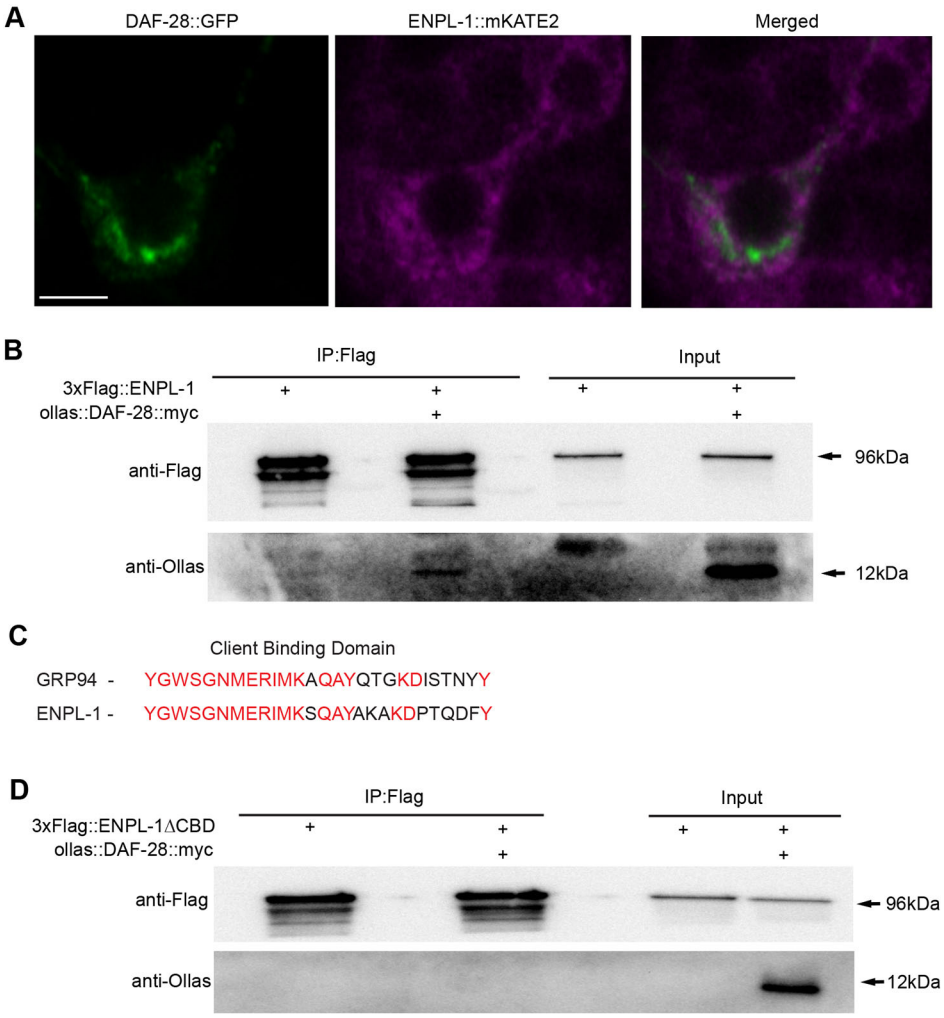

Fig. 6. ENPL-1 binds to proinsulin via the client binding domain. (A) Representative confocal images of amphid neurons in adult animals co-expressing DAF-28::GFP and ENPL-1::mKate2. Merged panel shows co-localization of both tagged proteins ($n \geq 10$). (B) Co-immunoprecipitation experiments with anti-Flag affinity beads from lysates of adult animals expressing 3xFlag::ENPL-1 and 3xFlag::ENPL-1 with OLLAS::DAF-28::MYC followed by western blot analysis. Inputs from every strain used in the analysis were used as a loading control. The experiment was performed in triplicate. (C) Alignment of sequences within the client binding domain sequence of GRP94 and ENPL-1. Conserved amino acids are marked in red. (D) Co-immunoprecipitation experiments with anti-Flag affinity beads from lysates of the adult animals expressing 3xFlag::ENPL-1 (ΔCBD) with or without *rawEx11* (OLLAS::DAF-28::MYC) followed by western blot analysis. Inputs from every strain used in the analysis were used as a loading control. The experiment was performed in triplicate. Scale bar: 5 µm.

et al., 2016) drawn from our previous work, showing that worm *asna-1* positively regulates DAF-28 secretion. This study led to the identification of a diabetic phenotype in murine ASNA-1/TRC40 knockdown animals. Thus, investigations in worms using DAF-28 secretion as an output will have substantial relevance for understanding insulin metabolism. Similarities of the functions between *C. elegans* and mammalian insulin show that study of DAF-28 control is relevant for human insulin biology and provides meaningful implications for understanding the role of insulin in the mammalian cells.

The maturation of pro-DAF-28 to the active form is analogous to the process for mammalian insulin (Li et al., 2003). Functional analysis has highlighted the RXXR sequence in DAF-28, where a proprotein convertase cleaves the proinsulin. *daf-28(sa191)* mutants, in which the RXXR is mutated to RXXC, form dauers in a semi-dominant manner, because the PERK (PEK-1) arm of the UPR pathway is cell-autonomously activated leading to ASI-specific phosphorylation of eIF2α (Kulalert and Kim, 2013). A later study identified the proprotein convertase to be KPC-1, as mutants failed to process DAF-28::GFP via the RXXR site. In *kpc-1* mutants, the migration pattern of DAF-28::GFP was altered (Hung et al., 2014). Our analysis, with a small double epitope-tagged DAF-28, which is of a similar size to wild-type DAF-28, confirms that this insulin is processed by *kpc-1*.

One of the main functions of GRP94 is to maintain ER homeostasis in the cell (Eletto et al., 2010; Mao et al., 2010; Marzec et al., 2012). It has been shown that GRP94 is one of the main targets of the ER stress response (Marzec et al., 2012). Consistently, in worms, depletion of *enpl-1* activity resulted in increased ER stress (Natarajan et al., 2013). We asked whether the defect in insulin secretion observed in *enpl-1* mutants is the main consequence of the high ER stress. Interestingly, a previous study has shown that mutants for of one of the UPR^{ER} branches, IRE-1/XBP-1, results in high ER stress and causes a defect in insulin secretion (Safra et al., 2013). Their study using DAF-28::GFP indicated that *ire-1* mutants displayed accumulation of DAF-28::GFP in the ER that is present only in neuronal cell bodies and no DAF-28::GFP reached the axons. This block consequently led to a lack of DAF-28::GFP secretion. Our analysis shows that the effect of the *enpl-1* mutation is different even though ER stress is high. The mutants are not blocked in DAF-28::GFP transport from the ER in the cell body to the dendrites and axons, suggesting that the ER stress is not a cause of the defective DAF-28::GFP secretion in *enpl-1(−)* animals. The neuronally expressed spliced form of XBP-1 has decreased ER stress by its ability to promote overexpression of ER chaperones. This leads to the activation of UPR^{ER} in neuronal and non-neuronal cells, leading to the rescue stress resistance (Taylor and Dillin, 2013). Furthermore, the same strain has been reported to rescue the *daf-28(sa191)* dauer mutant phenotype, by boosting IIS activity likely via improved folding and secretion of DAF-28 (Klabonski et al., 2016). As we report in this

Development (2020) 147, dev190082. doi:10.1242/dev.190082

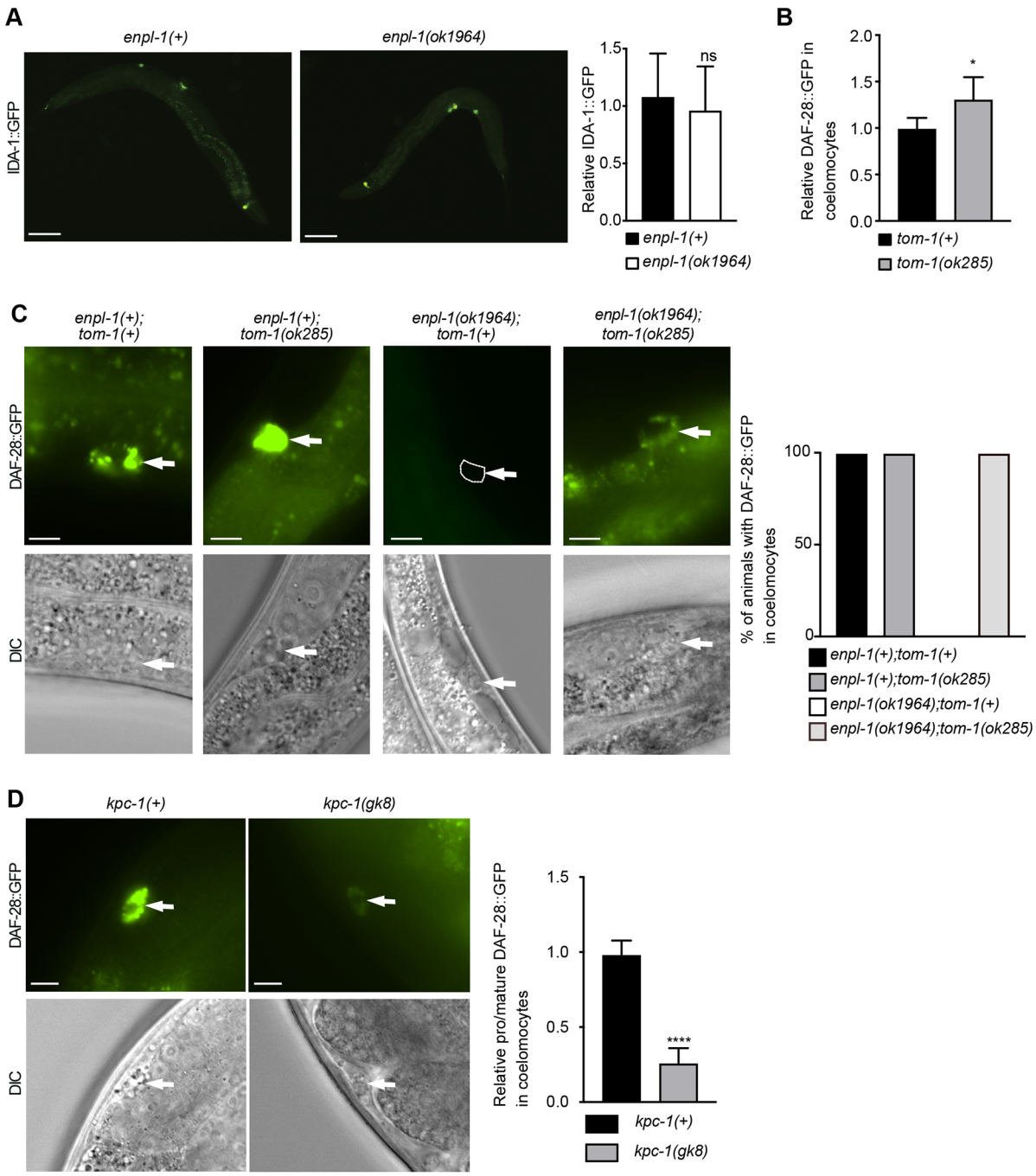

Fig. 7. Unregulated DCV release bypasses the secretion block of *enpl-1* mutants. (A) Representative fluorescence images of adult *enpl-1(+)* animals and *enpl-1(ok1964)* mutants expressing IDA-1::GFP. Quantification shows relative IDA-1::GFP fluorescence measured in head neurons, normalized to the *enpl-1(+)* strain, mean±s.d. ($n \geq 15$). Statistical significance was determined using the two-tailed *t*-test; ns, not significant. The experiment was performed in triplicate. (B) Quantification shows relative DAF-28::GFP fluorescence in coelomocytes, normalized to the *tom-1(+)* strain, mean±s.d. ($n \geq 15$). Statistical significance was determined using the two-tailed *t*-test (*$P<0.05$). The experiment was performed in triplicate. (C) Representative fluorescence and DIC images of adult *enpl-1(+);tom-1(+)*, *enpl-1(+);tom-1(ok285)*, *enpl-1(ok1964);tom-1(+)* and *enpl-1(ok1964);tom-1(ok285)* animals expressing DAF-28::GFP. White arrows indicate localization of coelomocyte in each animal. Dashed line shows DAF-28::GFP-negative coelomocyte. Quantification shows percentage of animals in which DAF-28::GFP is localized to coelomocytes ($n \geq 15$). (D) Representative fluorescence and DIC images of adult *kpc-1(+)* animals and *kpc-1(gk8)* mutants expressing DAF-28::GFP. White arrows indicate DAF-28::GFP-positive coelomocytes. Quantification shows relative DAF-28::GFP fluorescence in coelomocytes, normalized to the *kpc-1(+)* strain, mean±s.d. ($n \geq 15$). Statistical significance was determined using the two-tailed *t*-test (****$P<0.0001$). The experiment was performed in triplicate. Scale bars: 100 µm in A; 10 µm in C,D.

study, reduction of ER stress by the overexpression of XBP-1s did not improve the insulin secretion phenotype of *enpl-1* mutants.

In our study, we show that ENPL-1 interacts with pro-DAF-28/proinsulin and that its activity is essential for DAF-28/insulin secretion. Furthermore, increased ENPL-1 levels are sufficient to elevate secretion of DAF-28/insulin. Our results, together with results presented by Ghiasi et al. (2019), are not in agreement with a study that indicated the conditional pancreatic knockdown of

Development (2020) 147, dev190082. doi:10.1242/dev.190082

GRP94 resulted in increased insulin content, increased insulin secretion and increased mRNA levels of insulin genes (*ins-1* and *ins-2*) (Kim et al., 2018).

The analysis of the binding of ENPL-1 to pro-DAF-28 also showed that this interaction was important to ensure stable levels of pro-DAF-28. We expressed epitope-tagged DAF-28 using a multi-copy transgene that promoted high levels of the mRNA and protein. The ability of epitope tagged DAF-28 to force *daf-7/TGFBeta* dauers to exit the dauer state at 25°C was similar to the effects of overexpressed untagged DAF-28 (Kao et al., 2007) and indicated that *ollas::daf-28::myc* was functional. The lowered levels of *ollas::daf-28::myc* from the same transgene in *enpl-1* mutants indicated that binding to ENPL-1 protected DAF-28 from degradation. It is unlikely that increased accumulation of pro-DAF-28 by itself provides a signal for degradation, as levels of unprocessed DAF-28 were high in *kpc-1* mutants, which lack the proprotein convertase. This analysis indicates that one role for ENPL-1 could be to protect pro-DAF-28 from degradation before it reaches the immature DCV, in which it would be cleaved by KPC-1. Alternatively, the role of ENPL-1 might be to promote the proteolytic activity of KPC-1 by presenting the RXXR cleavage site of pro-DAF-28 in the proper orientation to the KPC-1 convertase.

Our studies also indicate that DAF-28::GFP likely reaches the DCVs in *enpl-1* mutants, as the block is bypassed in the *tom-1;enpl-1* double mutant. TOM-1 negatively regulates the release of neuropeptides from DCVs by blocking the fusion of DCVs to the cell membrane (Gracheva et al., 2007a,b; McEwen et al., 2006), which results in unregulated DCV release in the mutants. *tom-1(−)* lack the inhibitory function and display increase in DAF-28::GFP secretion (Lee et al., 2011). DAF-28::GFP secretion was restored in *enpl-1;tom-1* double mutants. This analysis first indicates that insulin reaches DCVs in *enpl-1* mutants, and second, that the defect is likely related to DCVs as *tom-1* only works in DCVs. In addition, we show that unprocessed insulin can be secreted, which strengthens our observation that the content of DCVs is affected in *enpl-1* mutants, preventing biologically active, mature DAF-28/insulin from being secreted. However, when the secretion block is challenged with *tom-1* mutants, the pro-DAF-28/proinsulin secretion is partly rescued.

Numerous studies have shown that ER resident proteins, such as GRP94, GRP78 and PDI, can translocate into different subcellular compartments in which they can function (Frasson et al., 2009; Patel et al., 2013; Shim et al., 2018; Sun et al., 2006; Takemoto et al., 1992; Tsai et al., 2001; Turano et al., 2002). Our study shows that some ENPL-1 can be found in the cytosol. This could be explained by the fact that ENPL-1 has, at the C-terminus, a form of an ER retention signal. However, the ER retention sequence of ENPL-1 (HSEL), is not a classical ER retention sequence (KDEL), but it is a weaker version, although still functional in retaining ER-resident proteins to the ER (Hirate and Okamoto, 2006). This observation, together with the fact that ENPL-1::sfGFP can be observed in the dendrites and axon of neurons that do not contain rough ER (Rolls et al., 2002), indicates additional post-ER localization of the protein. Furthermore, mammalian GRP94 has been demonstrated in several studies to have roles outside the ER lumen (Frasson et al., 2009; Patel et al., 2013). A notable example of this function is the role of GRP94 acting in plasma membranes to maintain proper levels of the oncogene HER2 at the cell membranes in HER2-overexpressing breast cancer cell lines. Inhibition of GRP94 disrupts HER2-stimulated signaling cascades (Patel et al., 2013). The localization of GRP94 both to the plasma membrane and to the ER lumen is phylogenetically conserved and not just a feature of mammalian GRP94 homologs (Robert et al., 1999).

GRP94 interacts with its client proteins via a C-terminal CBD. This region is well conserved in worm ENPL-1 and the crucial GNMER residues in the region required for client protein binding are perfectly conserved (Wu et al., 2012). We found that pro-DAF-28 binding to ENPL-1 requires the CBD as binding is not observed in an ENPL-1 variant deleted for this region. This matches the prediction of Ghiasi et al. that human proinsulin likely binds to this region (Ghiasi et al., 2019). The correspondence between the predicted human insulin binding to the CBD in GRP94 and our studies with GRP94/pro-DAF-28 again show that the study of DAF-28 in worms is relevant to human insulin biology. The 3xFlag::ENPL-1$^{\Delta CBD}$ protein is produced by the transgene at levels similar to its undeleted counterpart. Deletion in the CBD region in mouse GRP94 does not affect dimerization and the intrinsic ATPase activity of GRP94 (Wu et al., 2012), indicating that this deletion will not have a significant effect on the overall structure of ENPL-1. We therefore think it is unlikely that the 3xFlag::ENPL-1$^{\Delta CBD}$ protein is non-functional because of structural defects.

Here, we demonstrate that ENPL-1 regulates insulin processing and insulin secretion in *C. elegans* and that it acts at the level of insulin availability. Our study shows that proinsulin requires ENPL-1 for its proper cleavage and maturation, giving novel information of the role of ENPL-1 in the animal. A deeper understanding of how the insulin is processed and which protein complexes are associated with that mechanism might further contribute to the design of new drugs to target metabolic diseases.

MATERIALS AND METHODS

Plasmids

The double-tagged *daf-28* was made by inserting the OLLAS tag (SGFANELGPRLMGK) in the genomic DAF-28 coding region after the glycine residue in the FKAEG sequence of the protein. The Myc tag (EQKLISEEDL) was inserted just N-terminal to the stop codon of the gene. The hybrid double-tagged gene was synthesized (Genscript) as a NheI-KpnI fragment and cloned downstream of the *daf-28* promoter to replace the untagged *daf-28* coding region in pVB298 (Kao et al., 2007) to yield pAP2. Three transgenic lines bearing Ex[pAP2+Pmyo-3::mCherry] were generated in N2 animals by co-injection of 100 µg/ml of pAP2 together with Pmyo-3:mcherry 50 µg/ml. The transgenic line rawEx11, which produced the highest levels of protein as determined by western blot analysis, was used for further analysis.

C. elegans genetics and maintenance

Worms, males and hermaphrodites, were maintained under standard conditions at 20°C on nematode growth media (NGM) plates unless otherwise stated. N2 is the wild-type parent for all the strains in the study. The *svIs69* transgenic worms expressing daf-*28::*gfp have been previously described (Kao et al., 2007). The single copy 3xFlag::ENPL-1*(knuSi222)* was created using the MosSCI system (Frøkjær-Jensen et al., 2014). The insertion of the transgene was at the *ttTi5605* locus in chromosome 4. The 3xFlag sequence was inserted after the signal sequence of ENPL-1. 3xFlag::ENPL-1(ΔCBD) with an in-frame deletion of the CBD (deleted peptide sequence: YGWSGNMERIMKSQAYAKAKDPTQDFYA) was inserted using MosSCI technology at the *cxTi10882* site on chromosome 2 to generate *knuSi430*. The knock-in strains ENPL-1::mKATE2:*enpl-1(syb698)* and ENPL-1::sfGFP: *enpl-1(syb594)* were generated using Crispr-CAS9 technology. mKATE2 and sfGFP were introduced by genome editing N-terminal to the coding region for the final four amino acids, HSEL, of ENPL-1. In both cases, a flexible linker (encoding GASGASAS) was introduced just upstream of the fluorescence tags. The remaining strains *enpl-1(ok1964)* (backcrossed eight times with N2 and then used for this study), *daf-7(e1372)*, *kpc-1(gk8)*, *tom-1(ok285)*, *daf-16(mgDf50)*, *xbp-1(tm2457)* and the transgenic strains *xbp-1s(uthIs270)*,

Development (2020) 147, dev190082. doi:10.1242/dev.190082

daf-16::gfp(zIs356), *ida-1::gfp(inIs181;inIs182)* and *otIs356* expressing pan neural nuclear RFP were obtained from the *Caenorhabditis* Genetics Center (University of Minnesota). ANF::GFP (*oxIs180*)-expressing worms were a kind gift from Prof. Eric Jorgensen (University of Utah, USA). *enpl-1(tm3738)* mutants were a kind gift from the Shohei Mitani lab (Tokyo Women's Medical University, Japan) and the National Bioresource Project (Tokyo, Japan). *enpl-1(ok1964)* and *enpl-1(tm3738*) were maintained in trans to the balancer *nT1(qIs51)*.

Antibodies and western blotting

For experiments with extrachromosomal transgenic lines, 600 to 1000 animals were handpicked and washed with M9 buffer. For experiments with integrated lines, wild-type or mutants, animals were directly washed from the plate using M9. Worms were lysed in Next Advance Bullet Blender Homogenizer in buffer containing 10 mM Tris-HCl (pH 7.4), 150 mM NaCl, 5 mM EDTA, 0.5% NP40 (between 80 µl and 200 µl) using 0.2 mm stainless steel beads for 3 min at 4°C, followed by centrifugation at 14,000 rpm (18,400 ***g***) for 20 min at 4°C. Protein estimation was conducted using the BCA assay. Lysates were boiled with a 1× loading buffer containing SDS and β-mercaptoethanol. To detect proinsulin and insulin, lysates were separated by electrophoresis through 12.5% gels followed by 90 min wet transfer onto PVDF membranes. For analysis of other proteins, Mini-Protean TGX stain-free gradient precast gels (Bio-Rad) were used with Tris/Glycine/SDS Buffer (Bio-Rad) and Trans-Blot Turbo Transfer System Transfer pack membranes (Bio-Rad) for transfer to PVDF membranes. Proteins were detected using the following antibodies: anti-GFP [3H9, ChromoTek, RRID: AB_10773374, Cat# 3h9-100, LOT# 80626001AB, dilution: 1:1000], anti-GRP94 [9G10, Santa Cruz Biotechnology, RRID: AB_627676, Cat# sc-32249, LOT# K2717, dilution: 1:1000], anti-Flag [M2, Sigma-Aldrich, RRID: AB_262044, Cat# F1804, LOT# SLCD3990, dilution: 1:1000,] anti-tubulin [Sigma-Aldrich, RRID: AB_477579, Cat# T5168, LOT# 00000089494, dilution: 1:5000], anti-RME-1 [5G11, Developmental Studies Hybridoma Bank, RRID: AB_10571460; Cat# RME1, concentration: 0.5 µg/ml], anti-OLLAS [L2, Novus Biologicals, RRID: AB_1625980, Cat# NBP1-06713SS, dilution: 1:1000], anti-Myc [9E1, ChromoTek, RRID: AB_2631398, Cat# 9e1-100, LOT# 70117003AB, dilution: 1:1000]. The secondary antibodies, used at a dilution of 1:5000, were HRP conjugated: goat anti-rat [GE Healthcare Life Sciences, RRID: AB_772207, Cat# NA935, LOT# 16918042], sheep anti-mouse [GE Healthcare Life Sciences, RRID: AB_772193, Cat# NA9310, LOT# 16921365] and donkey-anti-rabbit [GE Healthcare Life Sciences, RRID: AB_2722659, Cat# NA934, LOT# 9670531]. Supersignal West Femto detection reagent (Thermo Fisher Scientific) was used to generate a signal, which was detected using a LAS1000 machine (Fujifilm).

Co-immunoprecipitation

Worms were grown on the NGM plates for 4 days at 20°C and lysed as described above. Then 300-1000 µg of total protein lysates were added to 40 µl of anti-Flag magnetic beads (M8823, Sigma-Aldrich) and tumbled end-over-end for 1 h at 4°C. Beads were magnetically separated and washed 3× for 10 min with 500 µl of wash buffer [10 mM Tris-HCl (pH 7.4), 150 mM NaCl, 5 mM EDTA]. Proteins were eluted by resuspending the washed beads in 20 µl of 2× loading dye with β-mercaptoethanol, followed by heating for 10 min at 95°C. SDS PAGE was performed as described above.

Fluorescence microscopy

Embryos, larvae and 1-day-old adult animals were grown at 20°C on NGM plates and anesthetized in 2 mM levamisole. Worms were imaged using a Nikon Ni-E microscope, equipped with Hamamatsu Orca flash4.0 camera.

Insulin signaling and neuropeptide secretion assays

One-day-old adult animals carrying *daf-16::gfp*, *daf-28::gfp* and *anf::gfp* transgenes were grown at 20°C and anesthetized in 2 mM levamisole. Animals were imaged using a Nikon Ni-E microscope, equipped with a Hamamatsu Orca flash4.0 camera. Subcellular distribution of DAF-16::GFP was measured directly after preparing the slide to avoid stress conditions. DAF-28::GFP and ANF::GFP uptake was measured in the coelomocytes of adult worms.

Quantification of fluorescence in coelomocytes

GFP fluorescence from coelomocytes was measured using ImageJ software. Correlated total cell fluorescence was calculated using the equation CTFC=integrated density−(area of selected cell×mean fluorescence of background readings). The protocol for fluorescence quantification is available at: https://theolb.readthedocs.io/en/latest/imaging/measuring-cell-fluorescence-using-imagej.html. Pictures for control and mutant animals expressing DAF-28::GFP were collected on the same day for each analysis at the same exposure settings.

daf-7 dauer enhancement assay

The dauer enhancement assay of the *enpl-1(ok1964);daf-7(e1372)* and *daf-7(e1372),enpl-1(ok1964);daf-16(mgDf50)* animals was carried out at 15°C and the dauer exit assay of the *ollas::daf-28::myc*;*daf-7(e1372)* animals was carried out at 25°C. The resulting dauers were observed for the presence of dauer alae.

Confocal microscopy

One-day-old adult animals were anesthetized using 2 mM levamisole, mounted on 2% agarose pads and directly imaged. The fluorescence signal was analyzed at 488 nm, 555 nm and 647 nm using a confocal laser scanning microscope (LSM700, Carl Zeiss) with LD C-Apochromat 40x/1.1 W Corr objective. Image processing was performed using ZEN Lite (Carl Zeiss) software.

RNA extraction and quantitative RT-PCR (qPCR)

Worms were grown on the NGM plates for 4 days at 20°C. Worms were synchronized by allowing a mixed-stage worm suspension in M9 buffer to settle for 3 min and collecting the supernatant which contained embryos and L1 larva. These were placed on fresh NGM plates for 48 h to grow until the young adult stage. Worms were resuspended in 75 µL Nucleozol (Macherey-Nagel). After lysis by three rounds of freeze/thaw (37°C and ethanol/dry ice), the RNA was extracted using the Aurum Total RNA Mini Kit (Bio-Rad). cDNA was synthesized using the iScript cDNA Synthesis Kit (Bio-Rad). qPCR was performed on a StepOnePlus Real-Time PCR System (Applied Biosystems) instrument using KAPA SYBR FAST qPCR Kit (Kapa Biosystems). The comparative Ct method was used to analyze the results and the reference gene used for the analysis was *cdc-42*.

Membrane fractionation

Worms were grown at 20°C on NGM plates for 4 days and harvested from the plate using M9 buffer. Worms were washed 3× using M9 buffer and lysed in Next Advance Bullet Blender Homogenizer, in 400 µl extraction buffer containing 50 mM Tris (pH 7.2), 250 mM sucrose, 2 mM EDTA with protease/phosphatase inhibitor cocktail (HALT, #1861281 Thermo Fisher Scientific). The lysates were cleared of carcasses by centrifugation at 2900 ***g*** at 4°C for 20 min. The supernatant was collected, resuspended to a volume of 2 mL with an extraction buffer, placed in polycarbonate centrifuge tubes (Beckman Coulter, 349622) and centrifuged for 60 min at 100,000 ***g*** at 4°C in a fixed-angle rotor. The supernatant fraction was concentrated to a volume of 20 µl using Vivaspin 2 Concentrators, 3000 MWCO (Sigma-Aldrich, VS0291). The pellet fraction was re-suspended in 20 µl of extraction buffer. Pellet and supernatant fractions were boiled using 2× loading dye with β-mercaptoethanol for 10 min at 95°C. SDS-PAGE was performed as described above. The anti-RME-1 antibody (Hadwiger et al., 2010) was used to show the proper separation of the membrane and cytoplasmic fractions, as it has been shown that RME-1 localizes to recycling endosome membranes (Grant et al., 2001).

DiI staining

DiI stain (1,1′-dioctadecyl-3,3,3′,3′-tetramethylindocarbocyanine perchlorate; D282, Thermo Fisher Scientific) was dissolved in DMSO to obtain a concentration of 2 mg/ml. The solution was diluted 1:200 with M9. One-day-old adult animals were placed into 150 µl of the solution and incubated for 3 h at room temperature. The worms were then transferred to fresh plates to de-stain for 1 h and then mounted on a 2% agarose slide with 2 mM levamisole. Animals were imaged using a confocal microscope as described above.

Cisplatin sensitivity assay

Cisplatin plates were prepared using MYOB media with 2% agar, and the drug was added at the concentration of 300 µg/ml. Cisplatin solution (Accord Healthcare AB) was added to the autoclaved media cooled to 56°C. Young adults were exposed to the cisplatin for 24 h and the death was scored by the absence of touch-provoked movement after stimulation with a platinum wire.

Pharyngeal pumping studies

The number of pharyngeal strokes per 20 s in 1-day-old adult animals was counted using a Leica MZFLIII dissecting microscope. A graph of recordings was plotted using Prism 7 software (GraphPad Software).

Fluorescent beads uptake assay

One-day-old adult animals of N2 or *enpl-1(ok1964)* mutants were incubated on NGM plates seeded with OP50 bacteria mixed with Fluoresbrites 0.2 µm multifluorescent microspheres (Polyscience, Inc.) at a ratio of 50:1 at 20°C. The mixture of bacteria and beads was added to the plates 20 h before use. The worms were incubated for 2 h at 20°C and then the micrographs of the treated worms were taken using the fluorescence microscope.

FM4-64 dye uptake assay

One-day-old adult animals were incubated in a solution of 0.4 mM FM4-64 dye (Molecular Probes) for 1 h at 20°C and the animals were then transferred to M9 buffer and incubated for 1 h at 20°C. Micrographs of the treated worms were taken using the fluorescence microscope.

Statistical analysis

Statistical analysis was performed using Prism 7 software (GraphPad Software). Statistical significance was determined using a two-tailed, unpaired Student's *t*-test. *P*-values <0.05 indicated statistical significance (*P<0.05, **P<0.01, ***P<0.001, ****P<0.0001).

Acknowledgements

We thank the *Caenorhabditis* Genetic Center (funded by National Institutes of Health Office of Research Infrastructure Programs P40 OD010440) and the National Bioresource Project for the Experimental Animal 'Nematode *C. elegans*' for providing strains, the Centre for Cellular Imaging at the University of Gothenburg and the National Microscopy Infrastructure, NMI (VR-RFI 2016-00968) for providing assistance in microscopy, and to members of the Simon Tuck and Marc Pilon labs for scientific discussions.

Competing interests

The authors declare no competing or financial interests.

Author contributions

Conceptualization: A.P.-F., G.K., P.N.; Methodology: A.P.-F., B.N., D.R., G.K.; Validation: A.P.-F., B.N., D.R., G.K.; Formal analysis: A.P.-F., G.K.; Investigation: A.P.-F., B.N., G.K.; Writing - original draft: A.P.-F., B.N., G.K., P.N.; Writing - review & editing: A.P.-F., D.R., G.K., P.N.; Visualization: A.P.-F., D.R., G.K.; Supervision: G.K., P.N.; Project administration: G.K., P.N.; Funding acquisition: P.N.

Funding

The work was supported by grants from Cancerfonden CAN 2018/664, ALF-agreement (ALFGBG-722971) between the Swedish government and the county councils.

Supplementary information

Supplementary information available online at
https://dev.biologists.org/lookup/doi/10.1242/dev.190082.supplemental

Peer review history

The peer review history is available online at
https://dev.biologists.org/lookup/doi/10.1242/dev.190082.reviewer-comments.pdf

References

Argon, Y. and Simen, B. B. (1999). GRP94, an ER chaperone with protein and peptide binding properties. *Semin. Cell Dev. Biol.* **10**, 495-505. doi:10.1006/scdb.1999.0320

Bell, G. I. and Polonsky, K. S. (2001). Diabetes mellitus and genetically programmed defects in β-cell function. *Nature* **414**, 788-791. doi:10.1038/414788a

Billing, O., Kao, G. and Naredi, P. (2011). Mitochondrial function is required for secretion of DAF-28/insulin in C. elegans. *PLoS ONE* **6**, e14507. doi:10.1371/journal.pone.0014507

Billing, O., Natarajan, B., Mohammed, A., Naredi, P. and Kao, G. (2012). A directed RNAi screen based on larval growth arrest reveals new modifiers of C. elegans insulin signaling. *PLoS ONE* **7**, 1-9. doi:10.1371/journal.pone.0034507

Calfon, M., Zeng, H., Urano, F., Till, J. H., Hubbard, S. R., Harding, H. P., Clark, S. G. and Ron, D. (2002). IRE1 couples endoplasmic reticulum load to secretory capacity by processing the XBP-1 mRNA. *Nature* **415**, 92-96. doi:10.1038/415092a

Christianson, J. C., Shaler, T. A., Tyler, R. E. and Kopito, R. R. (2008). OS-9 and GRP94 deliver mutant α1-antitrypsin to the Hrd1-SEL1L ubiquitin ligase complex for ERAD. *Nat. Cell Biol.* **10**, 272-282. doi:10.1038/ncb1689

DeFronzo, R. A. (2004). Pathogenesis of type 2 diabetes mellitus. *Med. Clin. North Am.* **88**, 787-835. doi:10.1016/j.mcna.2004.04.013

Eletto, D., Dersh, D. and Argon, Y. (2010). GRP94 in ER quality control and stress responses. *Semin. Cell Dev. Biol.* **21**, 479-485. doi:10.1016/j.semcdb.2010.03.004

Fielenbach, N. and Antebi, A. (2008). C. elegans dauer formation and the molecular basis of plasticity. *Genes Dev.*. **22**, 2149-2165. doi:10.1101/gad.1701508

Frasson, M., Vitadello, M., Brunati, A. M., La Rocca, N., Tibaldi, E., Pinna, L. A., Gorza, L. and Donella-Deana, A. (2009). Grp94 is Tyr-phosphorylated by Fyn in the lumen of the endoplasmic reticulum and translocates to Golgi in differentiating myoblasts. *Biochim. Biophys. Acta Mol. Cell Res.* **1793**, 239-252. doi:10.1016/j.bbamcr.2008.10.001

Frøkjær-Jensen, C., Davis, M. W., Sarov, M., Taylor, J., Flibotte, S., LaBella, M., Pozniakovsky, A., Moerman, D. G. and Jorgensen, E. M. (2014). Random and targeted transgene insertion in Caenorhabditis elegans using a modified Mos1 transposon. *Nat. Methods* **11**, 529-534. doi:10.1038/nmeth.2889

Ghiasi, S. M., Dahlby, T., Andersen, C. H., Haataja, L., Petersen, S., Omar-Hmeadi, M., Yang, M., Pihl, C., Bresson, S. E., Khilji, M. S. et al. (2019). Endoplasmic reticulum chaperone glucose-regulated protein 94 is essential for proinsulin handling. *Diabetes* **68**, 747-760. doi:10.2337/db18-0671

Gracheva, E. O., Burdina, A. O., Touroutine, D., Berthelot-Grosjean, M., Parekh, H. and Richmond, J. (2007a). Tomosyn negatively regulates CAPS-dependent peptide release at Caenorhabditis elegans synapses. *J. Neurosci.* **27**, 10176-10184. doi:10.1523/JNEUROSCI.2339-07.2007

Gracheva, E. O., Burdina, A. O., Touroutine, D., Berthelot-Grosjean, M., Parekh, H. and Richmond, J. (2007b). Tomosyn negatively regulates both synaptic transmitter and neuropeptide release at the C. elegans neuromuscular junction. *J. Physiol.* **585**, 705-709. doi:10.1113/jphysiol.2007.138321

Grant, B., Zhang, Y., Paupard, M.-C., Lin, S. X., Hall, D. H. and Hirsh, D. (2001). Evidence that RME-1, a conserved C. elegans EH-domain protein, functions in endocytic recycling. *Nat. Cell Biol.* **3**, 573-579. doi:10.1038/35078549

Hadwiger, G., Dour, S., Arur, S., Fox, P. and Nonet, M. L. (2010). A monoclonal antibody Toolkit for C. elegans. *PLoS ONE* **5**, e10161. doi:10.1371/journal.pone.0010161

Henderson, S. T. and Johnson, T. E. (2001). daf-16 integrates developmental and environmental inputs to mediate aging in the nematode Caenorhabditis elegans. *Curr. Biol.* **11**, 1975-1980. doi:10.1016/S0960-9822(01)00594-2

Hirate, Y. and Okamoto, H. (2006). Canopy1, a novel regulator of FGF signaling around the midbrain-hindbrain boundary in zebrafish. *Curr. Biol.* **16**, 421-427. doi:10.1016/j.cub.2006.01.055

Hua, Q.-X., Nakagawa, S. H., Wilken, J., Ramos, R. R., Jia, W., Bass, J. and Weiss, M. A. (2003). A divergent INS protein in Caenorhabditis elegans structurally resembles human insulin and activates the human insulin receptor. *Genes Dev.* **17**, 826-831. doi:10.1101/gad.1058003

Hung, W. L., Wang, Y., Chitturi, J. and Zhen, M. (2014). A Caenorhabditis elegans developmental decision requires insulin signaling-mediated neuron-intestine communication. *Development* **141**, 1767-1779. doi:10.1242/dev.103846

Kao, G., Nordenson, C., Still, M., Rönnlund, A., Tuck, S. and Naredi, P. (2007). ASNA-1 Positively Regulates Insulin Secretion in C. elegans and Mammalian Cells. *Cell* **128**, 577-587. doi:10.1016/j.cell.2006.12.031

Kapulkin, V., Hiester, B. G. and Link, C. D. (2005). Compensatory regulation among ER chaperones in C. elegans. *FEBS Lett.* **579**, 3063-3068. doi:10.1016/j.febslet.2005.04.062

Kass, J., Jacob, T. C., Kim, P. and Kaplan, J. M. (2001). The EGL-3 proprotein convertase regulates mechanosensory responses of Caenorhabditis elegans. *J. Neurosci.* **21**, 9265-9272. doi:10.1523/JNEUROSCI.21-23-09265.2001

Kim, M.-K., Kim, H.-S., Lee, I.-K. and Park, K.-G. (2012). Endoplasmic reticulum stress and insulin biosynthesis: a review. *Exp. Diabetes Res.* **2012**, 1-7. doi:10.1155/2012/509437

Kim, D.-S., Song, L., Wang, J., Wu, H., Gu, G., Sugi, Y., Li, Z. and Wang, H. (2018). GRP94 is an essential regulator of pancreatic β-cell development, mass, and function in male mice. *Endocrinology* **159**, 1062-1073. doi:10.1210/en.2017-00685

Klabonski, L., Zha, J., Senthilkumar, L. and Gidalevitz, T. (2016). A bystander mechanism explains the specific phenotype of a broadly expressed misfolded protein. *PLoS Genet.* **12**, e1006450. doi:10.1371/journal.pgen.1006450

Kulalert, W. and Kim, D. H. (2013). The unfolded protein response in a pair of sensory neurons promotes entry of C. elegans into Dauer diapause. *Curr. Biol.* **23**, 2540-2545. doi:10.1016/j.cub.2013.10.058
Lee, B. H., Liu, J., Wong, D., Srinivasan, S. and Ashrafi, K. (2011). Hyperactive neuroendocrine secretion causes size, feeding, and metabolic defects of C. elegans bardet-biedl syndrome mutants. *PLoS Biol.* **9**, e1001219. doi:10.1371/journal.pbio.1001219
Li, W., Kennedy, S. G. and Ruvkun, G. (2003). daf-28 encodes a C. elegans insulin superfamily member that is regulated by environmental cues and acts in the DAF-2 signaling pathway. *Genes Dev.* **17**, 844-858. doi:10.1101/gad.1066503
Maechler, P. (2013). Mitochondrial function and insulin secretion. *Mol. Cell. Endocrinol.* **379**, 12-18. doi:10.1016/j.mce.2013.06.019
Mao, C., Wang, M., Luo, B., Wey, S., Dong, D., Wesselschmidt, R., Rawlings, S. and Lee, A. S. (2010). Targeted mutation of the mouse Grp94 gene disrupts development and perturbs endoplasmic reticulum stress signaling. *PLoS ONE* **5**, e10852. doi:10.1371/journal.pone.0010852
Marzec, M., Eletto, D. and Argon, Y. (2012). GRP94: an HSP90-like protein specialized for protein folding and quality control in the endoplasmic reticulum. *Biochim. Biophys. Acta Mol. Cell Res.* **1823**, 774-787. doi:10.1016/j.bbamcr.2011.10.013
Maynard, J. C., Pham, T., Zheng, T., Jockheck-Clark, A., Rankin, H. B., Newgard, C. B., Spana, E. P. and Nicchitta, C. V. (2010). Gp93, the Drosophila GRP94 ortholog, is required for gut epithelial homeostasis and nutrient assimilation-coupled growth control. *Dev. Biol.* **339**, 295-306. doi:10.1016/j.ydbio.2009.12.023
McEwen, J. M., Madison, J. M., Dybbs, M. and Kaplan, J. M. (2006). Antagonistic regulation of synaptic vesicle priming by tomosyn and UNC-13. *Neuron* **51**, 303-315. doi:10.1016/j.neuron.2006.06.025
Nakae, J. U. N., Kido, Y., Accili, D., Berrie, N., Physicians, C. and Columbia, S. (2001). Distinct and overlapping functions of insulin and IGF-I receptors. *Endocr. Rev.* **22**, 818-835. doi:10.1210/edrv.22.6.0452
Natarajan, B., Gaur, R., Hemmingsson, O., Kao, G. and Naredi, P. (2013). Depletion of the ER chaperone ENPL-1 sensitizes C. elegans to the anticancer drug cisplatin. *Worm* **2**, 1-8. doi:10.4161/worm.24059
Norlin, S., Parekh, V. S., Naredi, P. and Edlund, H. (2016). Asna1/TRC40 controls β-cell function and endoplasmic reticulum homeostasis by ensuring retrograde transport. *Diabetes* **65**, 110-119. doi:10.2337/db15-0699
Ogg, S. and Ruvkun, G. (1998). The C. elegans PTEN homolog, DAF-18, acts in the insulin receptor-like metabolic signaling pathway. *Mol. Cell* **2**, 887-893. doi:10.1016/S1097-2765(00)80303-2
Ogg, S., Paradis, S., Gottlieb, S., Patterson, G. I., Lee, L., Tissenbaum, H. A. and Ruvkun, G. (1997). The Fork head transcription factor DAF-16 transduces insulin-like metabolic and longevity signals in C. elegans. *Nature* **389**, 994-999. doi:10.1038/40194
Orci, L., Ravazzola, M., Amherdt, M., Madsen, O., Perrelet, A., Vassalli, J. D. and Anderson, R. G. W. (1986). Conversion of proinsulin to insulin occurs coordinately with acidification of maturing secretory vesicles. *J. Cell Biol.* **103**, 2273-2281. doi:10.1083/jcb.103.6.2273
Ostrovsky, O., Ahmed, N. T. and Brodsky, J. L. (2009). The chaperone activity of GRP94 toward insulin-like growth factor II is necessary for the stress response to serum deprivation. *Mol. Biol. Cell* **20**, 1855-1864. doi:10.1091/mbc.e08-04-0346
Patel, P. D., Yan, P., Seidler, P. M., Patel, H. J., Sun, W., Yang, C., Que, N. S., Taldone, T., Finotti, P., Stephani, R. A. et al. (2013). Paralog-selective Hsp90 inhibitors define tumor-specific regulation of HER2. *Nat. Chem. Biol.* **9**, 677-684. doi:10.1038/nchembio.1335
Pierce, S. B., Costa, M., Wisotzkey, R., Devadhar, S., Homburger, S. A., Buchman, A. R., Ferguson, K. C., Heller, J., Platt, D. M., Pasquinelli, A. A. et al. (2001). Regulation of DAF-2 receptor signaling by human insulin and ins-1, a member of the unusually large and diverse C. elegans insulin gene family. *Genes Dev.* **15**, 672-686. doi:10.1101/gad.867301
Rhodes, C. J. and Alarcon, C. (1994). What β-cell defect could lead to hyperproinsulinemia in NIDDM? *Diabetes* **43**, 511-517. doi:10.2337/diab.43.4.511
Robert, J., Ménoret, A. and Cohen, N. (1999). Cell surface expression of the endoplasmic reticular heat shock protein gp96 is phylogenetically conserved. *J. Immunol.* **163**, 4133-4139.
Rolls, M. M., Hall, D. H., Victor, M., Stelzer, E. H. K. and Rapoport, T. A. (2002). Targeting of rough endoplasmic reticulum membrane proteins and ribosomes in invertebrate neurons. *Mol. Biol. Cell* **13**, 1778-1791. doi:10.1091/mbc.01-10-0514
Safra, M., Ben-Hamo, S., Kenyon, C. and Henis-Korenblit, S. (2013). The ire-1 ER stress-response pathway is required for normal secretory-protein metabolism in C. elegans. *J. Cell Sci.* **126**, 4136-4146. doi:10.1242/jcs.123000
Shen, X., Ellis, R. E., Lee, K., Liu, C.-Y., Yang, K., Solomon, A., Yoshida, H., Morimoto, R., Kurnit, D. M., Mori, K. et al. (2001). Complementary signaling pathways regulate the unfolded protein response and are required for C. elegans development. *Cell* **107**, 893-903. doi:10.1016/S0092-8674(01)00612-2
Shim, S. M., Choi, H. R., Sung, K. W., Lee, Y. J., Kim, S. T., Kim, D., Mun, S. R., Hwang, J., Cha-Molstad, H., Ciechanover, A. et al. (2018). The endoplasmic reticulum-residing chaperone BiP is short-lived and metabolized through N-terminal arginylation. *Sci. Signal.* **11**, eaan0630. doi:10.1126/scisignal.aan0630
Speese, S., Petrie, M., Schuske, K., Ailion, M., Ann, K., Iwasaki, K., Jorgensen, E. M. and Martin, T. F. J. (2007). UNC-31 (CAPS) is required for dense-core vesicle but not synaptic vesicle exocytosis in Caenorhabditis elegans. *J. Neurosci.* **27**, 6150-6162. doi:10.1523/JNEUROSCI.1466-07.2007
Steiner, D. F., Park, S.-Y., Støy, J., Philipson, L. H. and Bell, G. I. (2009). A brief perspective on insulin production. *Diabetes Obes. Metab.* **11**, 189-196. doi:10.1111/j.1463-1326.2009.01106.x
Sun, F.-C., Wei, S., Li, C.-W., Chang, Y.-S., Chao, C.-C. and Lai, Y.-K. (2006). Localization of GRP78 to mitochondria under the unfolded protein response. *Biochem. J.* **396**, 31-39. doi:10.1042/BJ20051916
Takemoto, H., Yoshimori, T., Yamamoto, A., Miyata, Y., Yahara, I., Inoue, K. and Tashiro, Y. (1992). Heavy chain binding protein (BiP/GRP78) and endoplasmin are exported from the endoplasmic reticulum in rat exocrine pancreatic cells, similar to protein disulfide-isomerase. *Arch. Biochem. Biophys.* **296**, 129-136. doi:10.1016/0003-9861(92)90554-A
Taylor, R. C. and Dillin, A. (2013). XBP-1 Is a cell-nonautonomous regulator of stress resistance and longevity. *Cell* **153**, 1435-1447. doi:10.1016/j.cell.2013.05.042
Thacker, C. and Rose, A. M. (2000). A look at the Caenorhabditis proprotein convertase family. *BioEssays* **22**, 545-553. doi:10.1002/(SICI)1521-1878(200006)22:6<545::AID-BIES7>3.0.CO;2-F
Thacker, C. Srayko, M. and Rose, A. M. (2000). Mutational analysis of bli-4/kpc-4 reveals critical residues required for proprotein convertase function in C. elegans. *Gene* **252**, 15-25. doi:10.1016/S0378-1119(00)00211-0
Tong, Y.-G. and Bürglin, T. R. (2010). Conditions for dye-filling of sensory neurons in Caenorhabditis elegans. *J. Neurosci. Methods* **188**, 58-61. doi:10.1016/j.jneumeth.2010.02.003
Tsai, B., Rodighiero, C., Lencer, W. I. and Rapoport, T. A. (2001). Protein disulfide isomerase acts as a redox-dependent chaperone to unfold cholera toxin. *Cell* **104**, 937-948. doi:10.1016/S0092-8674(01)00289-6
Turano, C., Coppari, S., Altieri, F. and Ferraro, A. (2002). Proteins of the PDI family: unpredicted non-ER locations and functions. *J. Cell. Physiol.* **193**, 154-163. doi:10.1002/jcp.10172
Wu, S., Hong, F., Gewirth, D., Guo, B., Liu, B. and Li, Z. (2012). The molecular chaperone gp96/GRP94 interacts with toll-like receptors and integrins via its C-terminal hydrophobic domain. *J. Biol. Chem.* **287**, 6735-6742. doi:10.1074/jbc.M111.309526
Zahn, T. R., Macmorris, M. A., Dong, W., Day, R. and Hutton, J. C. (2001). IDA-1, a Caenorhabditis elegans homolog of the diabetic autoantigens IA-2 and phogrin, is expressed in peptidergic neurons in the worm. *J. Comp. Neurol.* **429**, 127-143. doi:10.1002/1096-9861(20000101)429:1<127::AID-CNE10>3.0.CO;2-H
Zhang, W., Lilja, L., Mandic, S. A., Gromada, J., Smidt, K., Janson, J., Takai, Y., Bark, C., Berggren, P.-O. and Meister, B. (2006). Tomosyn is expressed in β-cells and negatively regulates insulin exocytosis. *Diabetes* **55**, 574-581. doi:10.2337/diabetes.55.03.06.db05-0015
Zheng, S., Chiu, H., Boudreau, J., Papanicolaou, T., Bendena, W., Chin-Sang, I. and Pessin, J. E. (2018). A functional study of all 40 Caenorhabditis elegans insulin-like peptides. *J. Biol. Chem* **293**, 16912-16922. doi:10.1074/jbc.RA118.004542

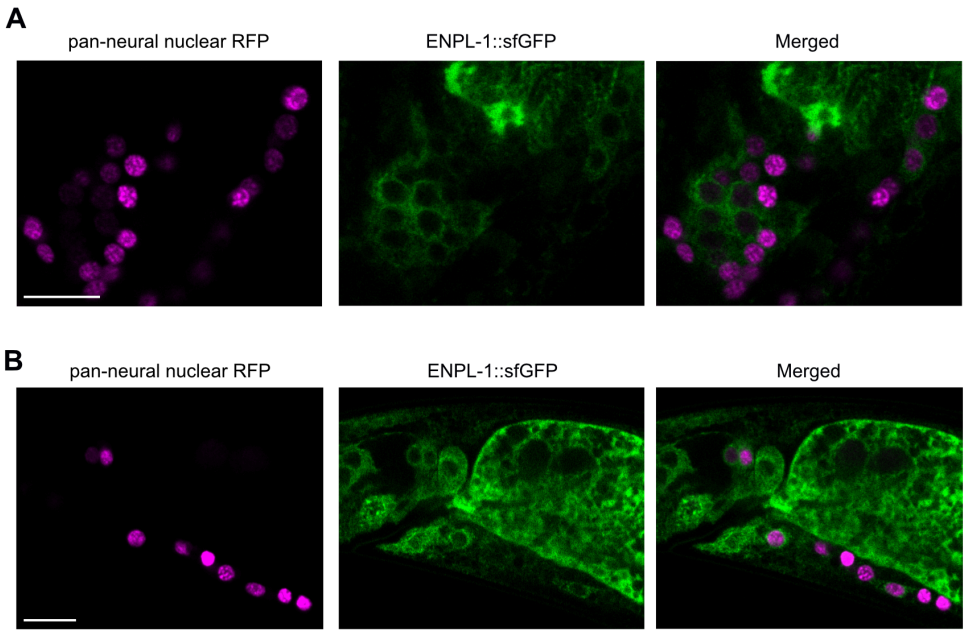

Fig. S1.

(A) Representative confocal images of adult animals co-expressing pan-neural nuclear RFP and ENPL-1::sfGFP in the lateral and ventral ganglia. Merged panel shows co-localization of both tagged proteins (n≥10). Scale bar: 10µm. (B) Representative confocal image of adult animals co-expressing pan-neural nuclear RFP and ENPL-1::sfGFP in ventral nerve cord. Merged panel shows co-localization of both tagged proteins (n≥10). Scale bar: 10µm.

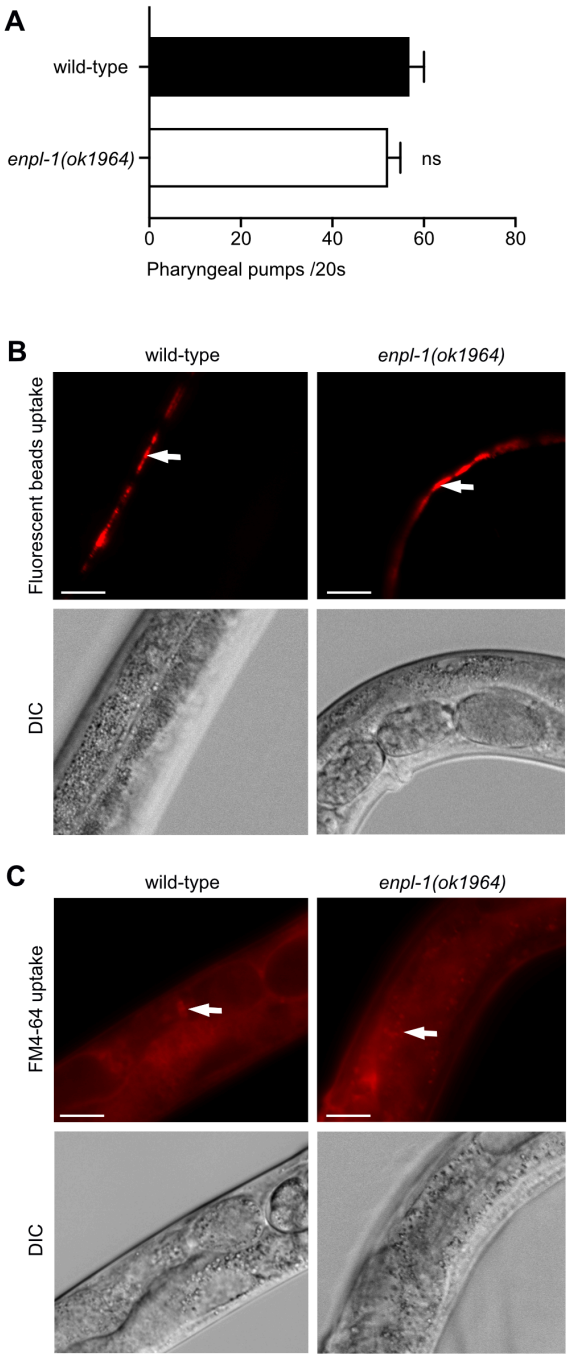

Fig. S2.

(A) Pharyngeal pumping rate in adult wild-type and *enpl-1(ok1964)* animals. Bars represent mean ± SD (n≥50). Statistical significance was determined by the two-tailed t-test. The experiment was performed in triplicate. (B) Fluorescence beads uptake of adult wild-type and *enpl-1(ok1964)* animals. White arrows indicate 0.2mm fluorescence beads in the intestinal lumen of treated animals (n=20). Scale bar: 25µm. (C) FM4-64 endocytosis of adult wild-type and *enpl-1(ok1964)* animals. White arrows indicate the FM4-64 uptake by the vesicles in the intestinal cells of treated animals (n=20). Scale bar: 25µm.

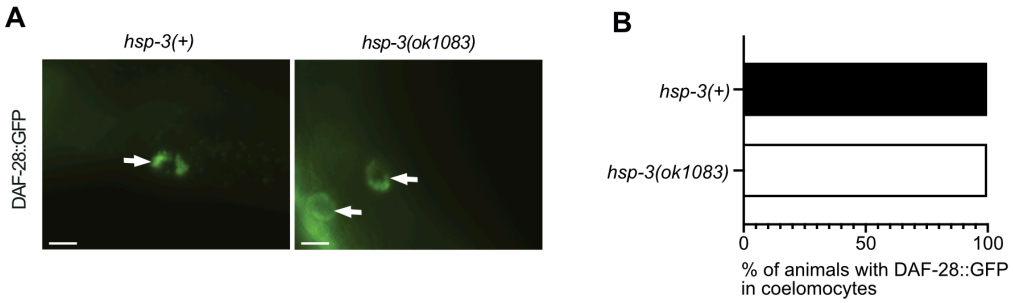

Fig. S3.

(A) Representative fluorescence images of adult *hsp-3(+)* animals and *hsp-3(ok1083)* mutants expressing DAF-28::GFP. White arrows indicate localization of DAF-28::GFP-positive coelomocytes (n≥15). Scale bar: 10µm. (B) Bars represent percentage of animals in which DAF-28::GFP is localized to coelomocytes (n≥15).

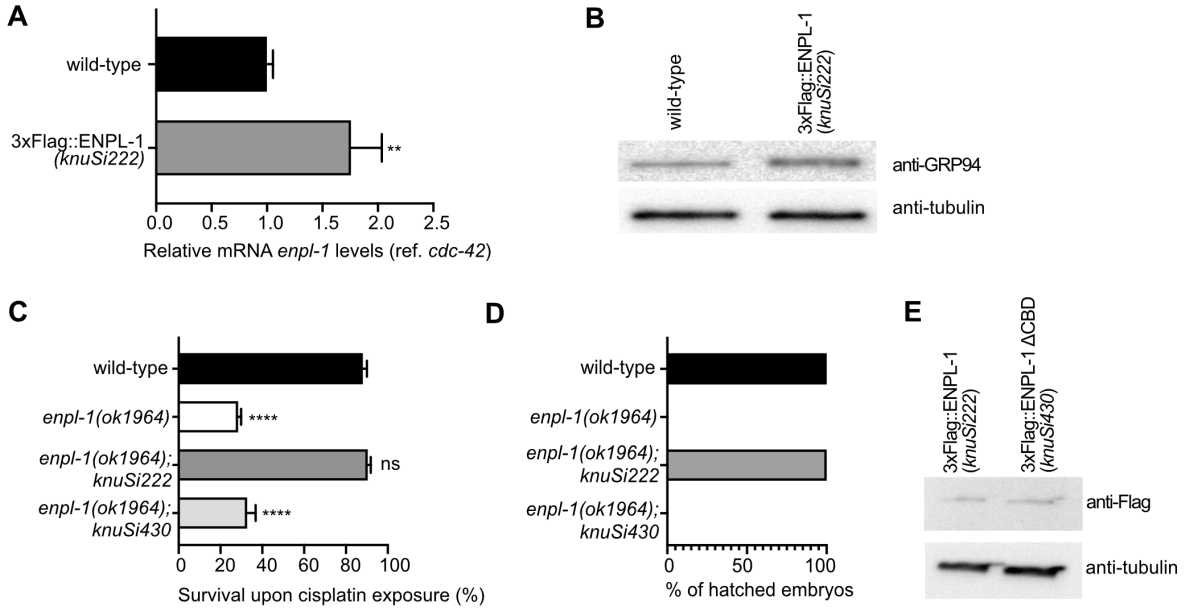

Fig. S4.

(A) Relative qPCR analysis of *enpl-1* expression in wild-type and 3xFlag::ENPl-1(*knuSi222*) animals. Statistical significance was determined by the two-tailed t-test (**p<0,01). Bars represent mean ± SD. *cdc42* was used as a normalizing control for the experiment. The experiment was performed in triplicate. (B) Western blot analysis of ENPL-1 in wild-type animals and 3xFlag::ENPL-1(*knuSi222*) expressing animals. Blots were probed with the anti-GRP94 antibody 9G10. Tubulin was used as a loading control. The experiment was performed in triplicate. (C) Quantification of survival of young adults after 24h exposure to 300µg/ml of cisplatin in wild-type animals, *enpl-1(ok1964)* mutants, *enpl-1(ok1964)* mutants carrying the *knuSi222* transgene (full-length ENPL-1) or *knuSi430* (CBD deleted ENPL-1). Statistical significance was determined by the two-tailed t-test (****p<0,0001). Bars represent mean ± SD (n≥50). The experiment was performed in triplicate. (D) Quantification of embryonic viability in wild-type animals, *enpl-1(ok1964)* mutants, *enpl-1(ok1964)* mutants carrying the *knuSi222* transgene (full-length ENPL-1) or *knuSi430* (CBD deleted ENPL-1). Bars represent percentage of hatched embryos (n≥50). (E) Western blot analysis of ENPL-1 in 3xFlag::ENPL-1(*knuSi222*) and 3xFlag::ENPL-1$^{\Delta CBD}$(*knuSi430*) expressing animals. Blots were probed with the anti-Flag antibody. Tubulin was used as a loading control. The experiment was performed in triplicate.

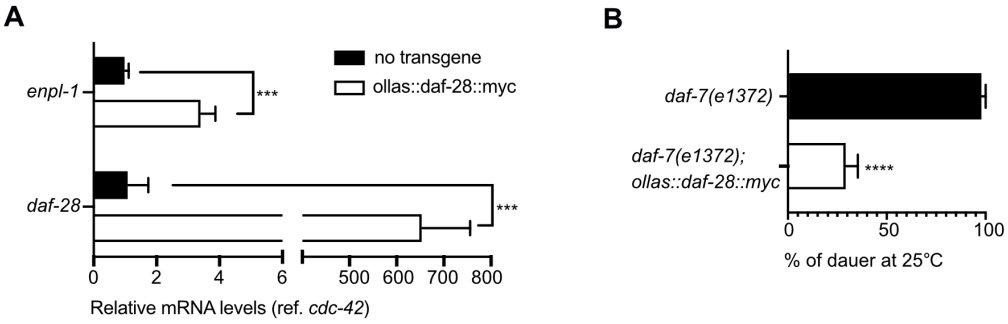

Fig. S5.

(A) Relative qPCR analysis of *enpl-1* and *daf-28* genes in non-transgenic animals and *rawEx11 (ollas::daf-28::myc)* bearing transgenic animals. Statistical significance was determined by the two-tailed t-test (***p<0,001). Bars represent mean ± SD. *cdc42* was used as a normalizing control for the experiment. The experiment was performed in triplicate. (B) *daf-7(e1372)* mutants with and without the transgene expressing *ollas::daf-28::myc* were analyzed for exit from the dauer state at 25°C after 96 hours. The transgene promoted dauer exit of *daf*-7 dauers raised at 25°C. Statistical significance was determined by the two-tailed t-test (****p<0,0001). Bars represent mean ± SD (n≥150). The experiment was performed in triplicate.